LBL-25410 c.2

Lawrence Berkeley Laboratory
UNIVERSITY OF CALIFORNIA

Materials & Chemical Sciences Division

RECEIVED
LAWRENCE
BERKELEY LABORATORY

AUG 5 1988

LIBRARY AND
DOCUMENTS SECTION

Chemical Reaction Rates via the Flux Correlation Function

J.W. Tromp
(Ph.D. Thesis)

May 1988

TWO-WEEK LOAN COPY
This is a Library Circulating Copy
which may be borrowed for two weeks.

LBL-25410 c.2

Prepared for the U.S. Department of Energy under Contract Number DE-AC03-76SF00098.

DISCLAIMER

This document was prepared as an account of work sponsored by the United States Government. While this document is believed to contain correct information, neither the United States Government nor any agency thereof, nor the Regents of the University of California, nor any of their employees, makes any warranty, express or implied, or assumes any legal responsibility for the accuracy, completeness, or usefulness of any information, apparatus, product, or process disclosed, or represents that its use would not infringe privately owned rights. Reference herein to any specific commercial product, process, or service by its trade name, trademark, manufacturer, or otherwise, does not necessarily constitute or imply its endorsement, recommendation, or favoring by the United States Government or any agency thereof, or the Regents of the University of California. The views and opinions of authors expressed herein do not necessarily state or reflect those of the United States Government or any agency thereof or the Regents of the University of California.

LBL-25410

Chemical Reaction Rates via the Flux Correlation Function

John William Tromp

(Ph.D. Thesis)

Department of Chemistry, University of California, and
Materials and Chemical Sciences Division, Lawrence Berkeley Laboratory,
Berkeley, California 94720

Chemical Reaction Rates via the Flux Correlation Function

John William Tromp

ABSTRACT

It is shown that the exact thermally averaged quantum mechanical rate constant of a chemical reaction can be obtained as the time integral of a reactive flux correlation function. This correlation function measures the time dependent correlation of reactive flux through a dividing surface separating reactants and products. The properties of the correlation function are then investigated, first for barrier passage problems in one dimension. The correlation function is obtained by enclosing the reacting system in a finite sized box, and determining the time dependence of the quantum operators by using the Heisenberg representation in terms of the discrete eigenvalues. All correlation functions have an initial positive lobe of width $\hbar\beta/2$ corresponding to initial direct flux, and may show longer time negative lobes corresponding to flux recrossing the dividing surface. Quantum transition state theory can be defined by using the correlation function to identify the short time quantum dynamics through the dividing surface.

Next the correlation functions are obtained for three different collinear reactions ($H + H_2$, $Cl + HCl$, and $F + H_2$), both quantum mechanically and classically. The features of the correlation functions can be interpreted in terms of the known dynamics of these reactions, and show the effects of direct tunneling, classical recrossing, and complex formation respectively.

Finally, a discrete Feynman path integral method is developed, where the multidimensional nature of the problem is treated through the introduction of an influence functional. The path integral is done by Monte Carlo and yields values of the correlation function for purely imaginary times. Real time values are obtained by analytic continuation. This method is tested on the collinear $H + H_2$ reaction, where it yields good results and can be readily extended to multidimensional systems.

ACKNOWLEDGEMENTS

First and foremost, I would like to thank my research director, Professor W.H. Miller for his patience, understanding, and direction over the last several years. I have learned much about science and how it is done during my time in the Miller group. I thank Professor H.F. Schaefer for advice and discussions. I would also like to thank the other members of the Miller group for help and encouragement during my years at Berkeley, and thanks to Cheryn Gliebe for all her help.

Thanks are due to various other friends, especially Roger Grev, Mike Colvin and Frank Eeckmann. I must also thank the other members of the Self Consistent Fielders Softball team for all the great seasons we have had, including that elusive championship season. Thanks to Leslie Carlin for everything. And finally, I am grateful to my parents for being my parents. Thanks Mom and Dad.

During some of my graduate career I was supported by the Natural Sciences and Engineering Research Council of Canada. This work was also supported by the National Science Foundation, and the Director, Office of Energy Research, Office of Basic Energy Sciences, Chemical Sciences Division of the U.S. Department of Energy under Contract Number DE-AC03-76SF00098.

TABLE OF CONTENTS

Acknowledgements i

Table of Contents ii

Chapter 1: Introduction 1

Chapter 2: Transition State Theory and the Reactive Flux Correlation Function 4

1. Introduction 4
2. A Qualitative Description of Transition State Theory 5
3. The Reactive Flux Correlation Function 7
4. The Classical Reactive Flux Correlation Function 15
5. The Free Particle Correlation Function 18
6. The Basis Set Method for One Dimensional Analysis 20
7. Quantum Transition State Theory in One Dimension 24
8. Comparison with Other Correlation Function Expressions 28
9. Separable Quantum Transition State Theory 33
10. Conclusions 35

Chapter 3: Collinear Reactions 36

1. Introduction 36
2. Theory and Method 37
   a. Quantum Calculations 37
   b. Classical Calculations 42
3. Results 44
   a. $H + H_2 \rightarrow H_2 + H$ 45

b. $Cl + HCl \rightarrow ClH + Cl$ 46

c. $F + H_2 \rightarrow FH + H$ 47

4. Concluding Remarks 49

Chapter 4: Path Integral Calculation of the Reactive Flux Correlation Function for Systems with Many Degrees of Freedom 50

1. Introduction 50

2. Theory and Computational Method 52

a. Path Integral Expression for the Flux Correlation Function 52

b. The Cartesian Reaction Hamiltonian and Influence Functional 59

c. Utility of the Influence Functional 65

d. Analytic Continuation Methods 67

3. Application to the Colinear $H + H_2$ System 70

4. Discussion 74

References 77

Tables 80

Figures 84

Chapter 1: Introduction

Transition state theory is a most useful theory of chemical reaction rates[1]. It is based on a simple assumption that is usually dynamically correct in the limiting case of low temperatures. The assumption is that the rate of a chemical reaction is determined entirely by the instantaneous dynamics through the tightest dynamical bottleneck separating reactants and products. If this assumption is not true, transition state theory still gives an upper bound to the rate constant[2,3], since any flux that recrosses the transition state region at later times was incorrectly included in the transition state theory prediction of the rate, and hence the latter must be too large.

However, transition state theory is conceptually based on classical mechanics. Its fundamental assumption, just outlined above, can only be stated with precision in classical mechanics where the concept of a classical trajectory is useful, and one can follow a trajectory to see whether or not it connects reactants and products[4]. The same cannot be done in quantum mechanics where the Heisenberg uncertainty principle invalidates the concept of a classical trajectory. However, quantum mechanics is the most fundamental dynamical theory needed to describe chemical phenomena. Moreover, as a practical matter at low temperatures where the fundamental assumption is most likely to be true classically, the quantum mechanical effect of tunneling through the barrier separating reactants and products is largest. Thus, even if the classical transition state theory is an upper bound to the exact classical rate, it vastly underestimates the true quantum mechanical rate constant. In the past there have been several attempts to put transition state theory

on a firm quantum mechanical foundation, but no attempt has been completely successful[5,6,7]. Thus in this thesis one of the principal goals is to understand quantum transition state theory: Can one state the assumptions of transition state theory with precision in quantum mechanics, and if so what language must be used, and what picture of chemical reactions does this lead to?

Closely related to this first theme is a parallel enterprise, which is the development of an efficient computational scheme for the calculation of ab initio chemical reaction rates. We assume the validity of the Born-Oppenheimer approximation, and further assume that quantum chemistry will be able to provide points on the electronic energy surface. Any quantum chemistry calculation has a finite cost, and so a method that minimizes this cost by only requiring potential surface information in the dynamically relevant region is preferred. This is of course the connection with transition state theory described above -- if transition state theory is correct then knowledge of the potential surface in the transition state region coupled with the appropriate dynamical theory yields the reaction rate.

Such an appropriate dynamical theory is the reactive flux correlation function which appears in the title of this thesis. The reactive flux correlation function was originally formulated by Miller, Schwartz and Tromp[8], who showed that the rate of a chemical reaction was given exactly in quantum mechanics by the integral over time of this correlation function. Initial calculation on one-dimensional barrier passage problems showed that the correlation function decayed to zero very quickly, typically in times less than $\hbar\beta$ (about 25 femtosec at T=300 K), indicating that dynamical methods valid for short times could be used to calculate the rate constant.

In this thesis two main avenues are explored. In the discrete basis set method the reacting system is enclosed in a box, and the resulting discrete eigenvalues and eigenvectors are obtained. Time evolution of any operator can then be obtained by

using the Heisenberg representation in this eigenstate basis. This is a short time method because eventually the presence of the walls starts to interfere with the dynamics that we are interested in. In calculations this can easily be separated from the "true" dynamics by making the artificial box bigger, and seeing if the correlation function is unchanged. Basis set methods have the obvious disadvantage that they are limited to systems with a few degrees of freedom, otherwise the basis set size becomes overwhelming. This method has been used to investigate the properties of the reactive flux correlation function in one-degree-of-freedom model systems, and in two-degree-of-freedom collinearly reacting systems.

A second approach is to use a discrete Feynman path integral representation of the propagator[9], and to perform the multidimensional path integrals by Monte Carlo. This approach can be extended to multidimensional systems governed by a general Hamiltonian where the influence functional for all other degrees of freedom can be evaluated exactly, yielding an effective one degree of freedom path integral calculation.

The outline of the thesis is as follows. In Chapter 2, the reactive flux correlation function formalism is described and related to the concepts of transition state theory by investigating the behavior of the correlation function for various one-dimensional potentials. In Chapter 3, three different collinear reactions ($H + H_2$, $Cl + HCl$, and $F + H_2$) are examined. This shows some of the range of behavior possible in a reacting system. Chapter 4 outlines the path integral method which could prove useful in the investigation of systems with many degrees of freedom, but has the limitation that it is accurate only for very short times, and is thus very similar in spirit to transition state theory.

Chapter 2: Transition State Theory and the Reactive Flux Correlation Function

1. INTRODUCTION

In this chapter we will discuss the dynamical basis of transition state theory, and show how transition state theory can be understood in terms of the reactive flux correlation function. The chapter begins with a qualitative introduction to classical transition state theory, and emphasizes the dynamical basis of what Wigner called the "fundamental assumption" of transition state theory[4], i.e. the assumption that the dynamics of reactions are direct so that if a trajectory crosses a dividing surface separating reactants and products it never returns. The variational aspect of classical transition state theory is also discussed[2,3]. After this general introduction, the quantum reactive flux correlation function is derived. The classical reactive flux correlation can then be obtained, by taking the classical limit, and the connection to transition state theory and the Wigner assumption easily made. The quantum version also allows a simple derivation of the usual practical version of quantum transition state theory[10], and clearly shows the dynamical assumptions involved. Next, some calculations of the reactive flux correlation function on a series of one-dimensional potentials using the basis set method are performed, and a way of stating the Wigner assumption quantum mechanically is proposed, leading to a new version of quantum transition state theory. Finally we compare the present reactive flux correlation function to alternative formulations, including the Kubo-transform correlation function previously obtained by Yamamoto[11,12], and we discuss the advantages of our formulation.

2. *A QUALITATIVE DESCRIPTION OF CLASSICAL TRANSITION STATE THEORY*

Aside from the "fundamental assumption" mentioned above, transition state theory is based on two other assumptions. These are the assumptions that the Born-Oppenheimer approximation is valid and that the reactants are maintained in thermal equilibrium. The first assumption, which is generally valid because of the mass difference between electrons and nuclei, is one of the basic assumptions of theoretical chemistry. It leads to the concept of an electronic potential surface that can be calculated by quantum chemistry, and allows us to consider a chemical reaction as a problem of only the nuclear dynamics on this potential surface.

The thermal equilibrium assumption is of a different nature. We can conceive of situations where the rate of collisional relaxation among reactants is slow compared to the difference in microcanonical rates, so that some reactant states become depopulated[13]. However, in such cases the experimental quantity being measured is not the thermal rate constant. Thus, this assumption amounts to requiring the experimentalist to guarantee that thermal equilibrium be maintained if a thermal rate constant is being measured.

There are many standard derivations of transition state theory[1,10]. In what follows we present a qualitative description of the principles involved. The conceptual assumption behind transition state theory is that for many chemical reactions the reaction rate will be determined entirely by the dynamics through a tight dynamical bottleneck separating reactants and products. To illustrate this, consider a simple model potential for barrier passage in one dimension such as the potential depicted in figure 1.

A chemical reaction occurs when a particle with sufficient energy crosses the barrier from left to right. Transition state theory introduces the mental construct of the dividing surface, a surface of F-1 dimensions where F is the dimensionality of

the system of interest. In our simple one-dimensional system, the dividing surface is of zero dimension, and corresponds to a point along the reaction co-ordinate. The transition state theory estimate of the rate constant then corresponds to the instantaneous flux through this dividing surface. Clearly the transition state theory rate constant depends on the dividing surface, as can be seen by considering the two different dividing surfaces shown in figure 1. The barrier maximum is at $s=0$, and this dividing surface is denoted by the solid vertical line. Another dividing surface denoted by the dashed vertical line is shown at $s_0 \neq 0$. At $s=0$, all points with energy greater than $V(0)$ contribute to the rate constant, while at $s=s_0$ all points with energy greater than $V(s_0)$ contribute. Thus, since $V(0) > V(s_0)$, the instantaneous estimate of the rate based on $s=s_0$ will be larger than that based on $s=0$. By considering the time evolved dynamics of points originating at $s=0$ and $s=s_0$ we can see how this arises: since $s=0$ is at the top of the barrier, all flux through $s=0$ is reactive, and if we follow a trajectory forever, it will never recross the dividing surface. On the other hand, it is clear that any trajectories originating at $s=s_0$ with energies between $V(s_0)$ and $V(0)$ and with initial momenta in the left direction will hit the barrier around $s \approx 0$ and at some later time recross the dividing surface at s_0. Following the trajectory over its entire course indicates its non-reactive nature.

This discussion illustrates the variational nature of transition state theory. The transition state theory estimate of the rate constant must be an upper bound to the true rate because if there is no recrossing transition state theory is exact. If recrossing occurs, transition state theory overestimates the rate. Thus, by varying the dividing surface until the transition state theory rate constant is minimized, the best estimate is obtained. The same sort of argument applies in the multidimensional situation. However, here the flux through a dividing surface depends not only on the barrier height, but also on the "width" of the potential in the other degrees of

freedom, with floppy orthogonal co-ordinates contributing more flux than tight ones. This will be seen more precisely after taking the classical limit of the quantum reactive flux correlation function, which is derived in the next section.

3. THE REACTIVE FLUX CORRELATION FUNCTION

The original derivation of the reactive flux correlation function formalism was presented by Miller, Schwartz and Tromp[8], based on a formally exact expression for the rate constant derived by Miller[7]. This derivation is completely rigorous, and starts with the well known expression for the rate constant in terms of a sum over squares of S-matrix elements between all states in the reactant and product channels. In what follows, a more heuristic derivation will be presented based not on the specific details of scattering theory, but on more general considerations of the time dependence of quantum projection operators which define reactants and products.

The idea is to obtain an exact quantum expression for the rate of a chemical reaction. The expression is to be based on the idea of a dividing surface as in transition state theory. In classical transition state theory the dividing surface serves to separate space into two regions, one region called reactants and another one called products. By simply measuring the instantaneous flux through this surface we obtain a zero time estimate of the rate constant.

The first step in the derivation will be to define two projection operators R and P that partition space into reactants and products. Between them, these two operators include all space, i.e. $P + R = 1$. The projector R must include the reactant channel out to infinite separation (between the reacting fragments), and P the product channel out to infinite separation (between the product fragments). Other than this, there is some arbitrariness to the definitions, since the concept of a reactant or product is not clearly defined in the interaction region. This arbitrariness is analogous to the variational nature of classical transition state theory, and so we also

expect that different choices of projection operator will be of different utility.

As an example of the utility of these chosen projection operators, consider a one dimensional barrier passage where the top of the barrier is located at $s=s_0$. The obvious classical transition state theory choice of dividing surface would be to place it at the top of the barrier, since this choice means that classical transition state theory is exact. To make the identical choice for our quantum projection operators, we can define

$$P_R = h(s_0-s) ,$$

$$P_P = h(s-s_0) , \tag{2.1}$$

where h is the step function

$$h(x) = 1, x>0 ,$$

$$h(x) = 0, x<0 . \tag{2.2}$$

For the general case it is now useful to define the eigenkets of these two operators, and also a Hamiltonian eigenstate basis. For the remainder of this discussion we will only use discrete labels in notation with the understanding that sums over discrete labels refer to both sums over discrete labels and integrals over continuous labels. Thus we define three types of states labelled by $|r\rangle$, $|p\rangle$, and $|\alpha\rangle$. The first two are eigenstates of the projection operators, and satisfy

$$R|r\rangle = |r\rangle ,$$

$$R|p\rangle = 0 ,$$

$$P|p\rangle = |p\rangle ,$$

$$P|r\rangle = 0\,, \tag{2.3}$$

while the third set are solutions to the time-independent Schrodinger equation

$$H|\alpha\rangle = E_\alpha|\alpha\rangle\,. \tag{2.4}$$

From equation (2.3) we can write R and P solely in terms of their eigenstates as

$$R = \sum_r |r\rangle\langle r|\,,$$

$$P = \sum_p |p\rangle\langle p|\,. \tag{2.5}$$

Now consider the expression we wish to obtain. We want to find the rate at which a thermal distribution of reactants becomes products. The rate is clearly a dynamical problem, and will be obtained by considering the time evolution of the system, but first we consider how to impose the requirement of thermal equilibrium. If we were starting from a scattering theory expression this would be easy, since the asymptotic states have a clearly defined energy, so the S-matrix square is just weighted by the Boltzmann distribution ($\exp(-\beta E_r)$). In our present notation the states $|r\rangle$ are clearly not eigenstates of the Hamiltonian --if they were they would display no time dependence, and there would be no rate to measure.

First consider the determination of the Boltzmann average of some observable. In the eigenstate basis, this is given by

$$\langle O\rangle_\beta = \sum_\alpha \exp(-\beta E_\alpha)\langle\alpha|O|\alpha\rangle\,. \tag{2.6}$$

Making use of the Schrodinger equation, this can be rewritten as

$$\langle O\rangle_\beta = \sum_\alpha \langle\alpha|\exp(-\lambda H)O\exp(-(\beta-\lambda)H)|\alpha\rangle\,, \tag{2.7}$$

where $0<\lambda<\beta$. The choice of λ is arbitrary, however it is convenient to make the choice $\lambda = \beta/2$, which gives the result

$$<O>_\beta = \sum_\alpha <\alpha|\exp(-\beta H/2)O\exp(-\beta H/2)|\alpha>$$

$$= \mathrm{tr}[\exp(-\beta H/2)O\exp(-\beta H/2)] , \tag{2.8}$$

where "tr" denotes a quantum mechanical trace

The reason for the symmetric choice is clear. By considering the Boltzmann probability operator to be divided into two equal Boltzmann amplitude operators, we can calculate quantum mechanical thermal amplitudes by including the operator $\exp(-\beta H/2)$. Any expectation value taken will be correctly weighted for a Boltzmann average, since the Boltzmann amplitude squared is the Boltzmann probability.

Thus, a thermalized reactant state is defined by

$$|r_\beta> = \exp(-\beta H/2)|r> . \tag{2.9}$$

Now consider the dynamical evolution of the thermalized reactant states. The time evolution of any state is given by the propagator (from the time-dependent Schrodinger equation), so the thermalized ket at some time t is given by

$$|r(\beta,t)> = \exp(-iHt/\hbar)\exp(-\beta H/2)|r> . \tag{2.10}$$

Defining the complex time variable t_c by

$$t_c = t-i\hbar\beta/2$$

allows the previous equation to be written as

$$|r(\beta,t)> = \exp(-iHt_c/\hbar)|r> . \tag{2.11}$$

The reaction amplitude at some time from the initial state $|r\rangle$ to some product state $|p\rangle$ is then simply obtained by the overlap with $\langle p|$

$$a_{rp}^{\beta}(t) = \langle p|\exp(-iHt_c/\hbar)|r\rangle \ . \tag{2.12}$$

Now we want to obtain the time dependent probability of overlap of any initial reactant state with any final product state, so we square and sum over reactant and product states to obtain

$$P_{RP}^{\beta}(t) = \sum_p\sum_r |a_{rp}^{\beta}(t)|^2$$

$$= \sum_p\sum_r \langle p|\exp(-iHt_c)|r\rangle\langle r|\exp(iHt_c^*)|p\rangle \ . \tag{2.13}$$

Finally, insertion of the resolution of the identity in terms of the eigenstate basis $(1=\sum_\alpha |\alpha\rangle\langle\alpha|)$ and rearrangement yields

$$P_{RP}^{\beta}(t) = \sum_\alpha\sum_p\sum_r \langle p|\alpha\rangle\langle\alpha|\exp(-iHt_c)|r\rangle\langle r|\exp(iHt_c^*)|p\rangle$$

$$= \sum_\alpha \langle\alpha|\exp(-iHt_c)(\sum_r |r\rangle\langle r|)\exp(iHt_c^*)(\sum_p |p\rangle\langle p|)|\alpha\rangle$$

$$= \mathrm{tr}[\exp(-iHt_c)R\exp(iHt_c^*)P] \ , \tag{2.14}$$

where we have made use of the definition of a quantum mechanical trace, and the definitions of R and P given by eqn (2.5).

This equation gives the time dependent conversion from reactant into product. The rate of conversion of reactant into product is related to the derivative of this expression. Recall earlier that the definition of reactant projection operator extended asymptotically to infinity in the reactant channel. Thus, after some initial transient, the expression defined by eqn (2.14) will attain a constant slope with time,

corresponding to a steady state flux of conversion from reactants to products. Thus except for a normalization factor, the rate is given by the long time limit of the time derivative of eqn (2.14).

Now consider the evaluation of the normalization factor. The expression just given is a generalized rate for conversion from reactants to products in terms of quantum number density. To obtain the chemical rate constant, we want the rate in reactant particle density. The reactant partition function Q is by definition the number of quantum states per particle, so its inverse is the correct normalization factor. A different approach is to compare the present expression with separable quantum transition state theory where it is exact, and the same normalization factor is obtained. (This is discussed more completely later in the chapter.) Thus, the expression for the rate is

$$k = \frac{1}{Q} \lim_{t \to \infty} \frac{d}{dt} P^{\beta}_{RP}(t) \ . \tag{2.15}$$

At this point it may appear that not much has been accomplished. The original goal was to obtain an expression that had some conceptual relationship to transition state theory, and we do have an expression that contains the concept of reactive flux through a dividing surface. However, unlike transition state theory where the rate is obtained as a zero time limit, the present expression requires the evaluation of the dynamics out to infinite time. The connection arises from the actual time behavior of eqn (2.15) where in practice the limiting slope is attained in short time. To see this we will finally derive the expression in terms of the reactive flux correlation function. Taking the explicit time derivative of eqn (2.15), we obtain

$$k = \lim_{t \to \infty} k_{eff}(t) \ , \tag{2.16}$$

where

$$k_{eff}(t) = \frac{1}{Q}\mathrm{tr}[\exp(-iHt_c/\hbar)\frac{i}{\hbar}[H,R]\exp(iHt_c^*/\hbar)P] \ .$$

For t = 0, the trace in eqn (2.16) is identically zero. This can be seen most easily by substituting P = 1 − R, and expanding the commutator. Cyclic permutation of one of the trace expressions leads to exact cancellation of all four terms. Thus eqn (2.16) can be written as

$$k = \frac{1}{Q}\mathrm{tr}[\exp(iHt_c/\hbar)\frac{i}{\hbar}[H,R]\exp(-iHt_c^*)P] \,|_{t=0}^{t=\infty}$$

$$= \int_0^\infty C_f(t)\, dt \ , \tag{2.17}$$

where

$$C_f(t) = \frac{d}{dt}\ \mathrm{tr}[\exp(iHt_c/\hbar)\frac{i}{\hbar}[H,R]\exp(-iHt_c^*)P] \ .$$

Taking the time derivative of the propagator as before leads to the final expression for $C_f(t)$:

$$C_f(t) = \mathrm{tr}[\exp(iHt_c/\hbar)F_R\exp(-iHt_c^*)F_P] \ , \tag{2.18}$$

where F_R , and F_P are defined by

$$F_P = \frac{i}{\hbar}[H,P] \ ,$$

$$F_R = \frac{i}{\hbar}[H,R] \ . \tag{2.19}$$

Now in eqn (2.1) a coordinate representation of the operators P and R was introduced. This selection corresponds to the concept of the dividing surface in transition state theory. Thus it is useful to explicitly evaluate the commutator for

this choice of projection operator. Since the potential is a function of only the coordinate s, it commutes with the step function, so we have

$$F_P = \frac{i}{\hbar}[\frac{p^2}{2m},h(s-s_0)]$$

$$= \frac{i}{\hbar}\frac{1}{2m}\{p[p,h(s-s_0)] + [p,h(s-s_0)]p\}$$

$$= \frac{i}{\hbar}\frac{\hbar}{i}\frac{1}{2}[\frac{p}{m}\delta(s-s_0) + \delta(s-s_0)\frac{p}{m}]$$

$$= F_R = F\,. \tag{2.20}$$

The reason for the notation is clear. The operator F measures the flux $\frac{p}{m}$ through a dividing surface located at $s = s_0$. Thus we see that we have obtained an expression for the rate constant of a reaction as the time integral of a flux autocorrelation function.

Yamomoto[11] has previously obtained an expression for the rate constant in terms of the time integral of a correlation function. His correlation function corresponds to performing an integral over all λ as defined in eqn(2.7) instead of just making the symmetric choice. The actual time behavior of these two correlation functions is different, although their integrals must agree. The advantages of the present formulation will be outlined in more detail in section 8.

4. *THE CLASSICAL REACTIVE FLUX CORRELATION FUNCTION*

At this point, it is useful to consider the classical limit of the reactive flux correlation function. The reason for this is that, as stated in the introduction, transition state theory is inherently based in classical mechanics. Thus, by taking the classical limit, we can identify precisely the correspondence between transition state theory and the reactive flux correlation function, at least in classical mechanics. Later this correspondence will be generalized to include the quantum situation as well. The classical expression is obtained from the corresponding quantum expression by replacing all operators with classical functions, and by replacing the quantum trace with a phase space average.

At this point we note that classical reactive flux correlation functions have been derived previously[14,15], and are especially useful in the study of reactions in solution. Trajectories that start in the reactant configuration rarely make it to the transition state region due to the high dimensionality of phase space. However, by starting trajectories in the transition state region they can be followed long enough to determine their reactive or nonreactive nature.

For convenience, we consider a situation where there are only two degrees of freedom. The extension to the multidimensional case is made by considering many degrees of freedom orthogonal to the reaction co-ordinate instead of the single one considered here. If s is the reaction coordinate and Q the coordinate orthogonal to it, then the classical expression for the reactive flux correlation function for a dividing surface at $s = s_0$ is

$$C_f^{CL}(t) = (2\pi\hbar)^{-2}\int ds_1 \int dp_1 \int dQ_1 \int dP_1 \exp[-\beta\{\frac{p_1^2}{2m} + \frac{P_1^2}{2m} + V(s_1,Q_1)\}]$$

$$\frac{p_1}{m}\,\delta(s_1-s_0)\,\delta(s(t)-s_0)\,\frac{p(t)}{m}\,, \tag{2.21}$$

where (p,P) are the momenta conjugate to (s,Q), and s(t) and p(t) are the values of s and p that have evolved classically from the initial conditions (s_1,p_1,Q_1,P_1). The presence of the delta function allows the integral over s_1 to be done immediately, giving

$$C_f^{CL}(t) = (2\pi\hbar)^{-1}\int dQ_1 \int dP_1 \exp[-\beta\{\frac{P_1^2}{2m} + V(s_0,Q_1)\}]$$

$$(2\pi\hbar)^{-1}\int dp_1\,\frac{p_1}{m}\exp[-\beta\frac{p_1^2}{2m}]\,\delta(s(t)-s_0)\,\frac{p(t)}{m}\,. \tag{2.22}$$

It is illustrative to consider this equation in the short time limit. In this limit s(t) and p(t) are given by a free particle trajectory (independent of Q_1 and P_1),

$$s(t) = s_0 + \frac{p_1}{m}\,t\,,$$

$$p(t) = p_1\,, \tag{2.23}$$

so that eqn (2.22) becomes

$$C_f^{CL}(t) = Q_{CL}^{\ddagger}\,(2\pi\hbar)^{-1}\int_{-\infty}^{\infty} dp_1 \exp[-\beta\frac{p_1^2}{2m}](\frac{p_1^2}{m})\delta(\frac{p_1}{m}t)\,, \tag{2.24}$$

where $Q_{CL}^{\ddagger}$ is the classical partition function of the activated complex on the dividing surface,

$$Q_{CL}^{\ddagger} = (2\pi\hbar)^{-1}\int dP_1 \int dQ_1 \exp(-\beta[\frac{P_1^2}{2m} + V(s_0,Q_1)])\,. \tag{2.25}$$

Since

$$\delta(\frac{p_1}{m}t) = |\frac{m}{p_1}|\delta(t)$$

and

$$(2\pi\hbar)^{-1} \int_{-\infty}^{\infty} dp_1 \exp(-\beta\frac{p_1^2}{2m}) \, |\frac{p_1}{m}| = 2\frac{kT}{h} ,$$

eqn (2.24) becomes

$$C_f^{CL}(t) = \frac{kT}{h} Q_{CL}^{\ddagger} \, 2 \, \delta(t) . \tag{2.26}$$

The analysis in the above paragraph shows that the classical correlation function will always have a short time, free-particle delta function at $t = 0$. If $s(t)$ is never equal to s_0 for $t > 0$, then eqn (2.26) is the complete classical correlation function -- which is just the statement that classical transition state theory is exact if no trajectories re-cross the dividing surface. If $s(t)$ does equal s_0 at some later time $t > 0$, then $p(t)$ will have the opposite sign of p_1 if this is the first recrossing time for this trajectory; if it is the second recrossing, $p(t)$ and p_1 will have the same sign, and so forth. Thus negative and the positive regions of $C_f(t)$ are identified as classical recrossing effects. In section 7 we will show how the quantum correlation function can be interpreted the same way.

5. *THE FREE PARTICLE CORRELATION FUNCTION*

Before continuing the general one dimensional result, one specific and important result will be obtained: that of $C_f(t)$ for a free particle in one dimension. It is most convenient to do this in a coordinate representation, where matrix elements of the flux operator and complex time propagator can be obtained explicitly.

Thus, using the fact that it can readily be shown that the coordinate representation of the flux operator (with dividing surface chosen at s = 0) is given by

$$<s|F|s'> = \frac{\hbar}{2im}[\delta'(s)\delta(s')-\delta(s)\delta'(s')] , \tag{2.27}$$

where $\delta'(s)$ is the derivative of the delta function allows (with some algebra) one to obtain the coordinate representation of the reactive flux correlation function:

$$C_f(t) = (\frac{\hbar}{2m})^2(\frac{\partial^2}{\partial s\partial s'}|<s'|\exp(-iHt_c/\hbar)|s>|^2$$

$$-4|\frac{\partial}{\partial s'}<s'|\exp(-iHt_c/\hbar)|s>|^2)|_{s'=s=0} . \tag{2.28}$$

Note that if the potential is symmetric about s=0, the second term of this equation is zero. This can be seen most easily by inserting an eigenstate basis resolution of the identity into this term:

$$\frac{\partial}{\partial s'}<s|\exp(-iHt_c/\hbar)|s'> = \int dE\frac{\partial}{\partial s'}<s'|E><E|s>\exp(-iEt_c/\hbar) . \tag{2.29}$$

The wavefunctions $<s|E>$ are of either g or u symmetry, so either the wavefunction or its derivative is zero at s = 0.

Now we know the explicit form of the free particle complex time propagator

$$<s'|\exp(iHt_c/\hbar|s> = (\frac{m}{2\pi i\hbar t_c})^{1/2}\exp[\frac{im}{2\hbar t_c}(s-s')^2] \ , \tag{2.30}$$

so substitution and evaluation of the partial derivative immediately gives the result

$$C_f^{FP}(t) = \frac{kT}{h}\frac{(\hbar\beta/2)^2}{[t^2 + (\hbar\beta/2)^2]^{3/2}} \ . \tag{2.31}$$

The integral of this correlation function can be done immediately, to give the rate and the result is kT/h. This is the same as the classical result, which is of course expected for the free particle situation. This function decays monotonically to zero with a width proportional to $\hbar\beta/2$. Thus, in the classical limit obtained either by letting $\hbar\rightarrow 0$, or by letting $\beta\rightarrow 0$ (infinite temperature), the width becomes zero, and the delta function at the origin described in the last section is recovered.

In quantum mechanics, $\hbar$ is finite, and so the correlation function does have a finite width. Thus, it is clear that in quantum mechanics transition state theory cannot be obtained by taking the zero time limit of the dynamics. However, the fundamental assumption of classical transition state theory, i.e. that no trajectories recross the divide surface for $t > 0$ can be restated to say that the assumption is that the dynamics are direct. In the quantum correlation function, this direct dynamics can be associated with the positive lobe of $C_f(t)$ about $t = 0$. However we see already that defining a version of transition state theory in quantum mechanics will be less obvious than in classical mechanics.

The broadening of the free particle correlation function in quantum mechanics is due to the uncertainty principle. A simple argument to show this is based on the energy-time uncertainty principle

$$\Delta E\cdot\Delta t \simeq \hbar \ .$$

The Boltzmann distribution implies a finite energy distribution of the order of $1/\beta$ so

the time distribution is of the order of $\hbar\beta$.

6. *THE BASIS SET METHOD FOR ONE-DIMENSIONAL ANALYSIS*

In this section the behavior of the one dimensional reactive flux correlation function will be presented for various one dimensional potentials. In one dimension the numerical evaluation of the correlation function can be done routinely, and so insight into the behavior of the correlation function can be developed.

For general one dimensional potentials explicit analytic results are not possible, so instead the correlation function is obtained using a basis set method. If $\{\phi_n(s)\}$ is some finite set of square integrable basis functions, the Hamiltonian can be diagonalized in this basis set to yield a set of eigenvalues $\{E_i\}$ and eigenfunctions $\{\psi_i(s)\}$. In this representation the trace becomes a sum over all eigenstates, and the expression for $C_f(t)$ can be written as

$$C_f(t) = \sum_{i,j} \exp[-\beta(E_i+E_j)/2]\cos[(E_i-E_j)t/\hbar]\,|\langle i|F|j\rangle|^2 , \tag{2.32}$$

where

$$|\langle i|F|j\rangle|^2 = |\int ds \int ds' \psi_i(s)^* \langle s|F|s'\rangle \psi_j(s')|^2$$

$$= (\frac{\hbar}{2m})^2 |\psi_i'(0)\psi_j(0) - \psi_i(0)\psi_j'(0)|^2 . \tag{2.33}$$

The expression for $C_f(t)$ can be directly integrated to yield $k_{eff}(t)$

$$k_{eff}(t) = \frac{1}{Q} \sum_{i,j} \exp[-\beta(E_i+E_j)/2] \frac{\sin[(E_i-E_j)t/\hbar]}{(E_i-E_j)/\hbar} |\langle i|F|j\rangle|^2 . \tag{2.34}$$

Although the formal limit is $k = \lim_{t\to\infty} k_{eff}(t)$, this limit does not exist as can be seen by noting the identity

$$\lim_{t\to\infty}\frac{\sin[(E_i-E_j)t/\hbar]}{E_i-E_j} = \pi\delta(E_i - E_j) \ . \tag{2.35}$$

Thus, any discrete basis set can never give the infinite time limit correctly. This is not a problem in practice because we do not want to take the infinite time limit of the expression, instead we want to follow the dynamics for only a short time, the duration for which $C_f(t)$ is non-zero. We want to use as small a basis as possible so the choice of basis set is very important. In initial calculations on one dimensional barrier problems a basis set of 1-d harmonic oscillator eigenfunctions centered on the top of the barrier was used. This basis set worked well for high temperatures where the tunneling correction was small, but low temperature results could not be obtained even with very large basis sets. Alternatively, excellent results were obtained by using a particle-in-a-box basis set, with very few basis functions needed to obtain excellent results. The basis set is defined by

$$\phi_n(s) = (\frac{2}{L})^{1/2}\sin\{\frac{n\pi}{L}(s-s_{min})\} \ , \tag{2.36}$$

where $L=s_{max}-s_{min}$, and s_{max}, and s_{min} are the limits of the box.

This difference in the utility of the basis functions was initially surprising, but can be rationalized. By using a particle-in-a-box basis set we are in effect solving a different dynamical problem --that of a particle confined to a box with a barrier in the middle. The true eigenstates of this problem are discrete since it is a bound state problem, and the basis set used is very efficient for solving the problem. Clearly the walls must have an effect on the correlation function because after a long enough time flux which originated at the dividing surface location must reflect off the walls of the box, and lead to a long time spurious contribution to $C_f(t)$. This recrossing has a well defined physical origin (the walls), and so its effect can be separated from the dynamics due to the potential of interest by simply moving the

walls further out. This leads to the reflection off the walls occurring at a longer time. This simple physical interpretation of the effect of the basis set is not clear when a harmonic oscillator basis set is used, since one cannot visualise physically what the long time behavior of $C_f(t)$ is due to.

Now consider specific examples of calculations for one dimensional systems. We first calculate $C_f(t)$ for the symmetrical Eckart barrier shown in figure 1, defined by

$$V(s) = V_0 \mathrm{sech}^2(s/a) , \tag{2.37}$$

where V_0 is the barrier height and a is the width of the barrier. The behavior of the tunneling correction Γ with respect to barrier height, barrier width, and temperature is a function of only two dimensionless parameters defined by

$$\alpha = \pi(2mV_0a^2/\hbar^2)^{1/2} . \tag{2.38a}$$

$$u = \hbar\beta(2V_0/a^2m)^{1/2} , \tag{2.38b}$$

with Γ defined implicitly as a correction to classical transition state theory by

$$kQ = \Gamma\frac{kT}{h}\exp(-\beta V_0) . \tag{2.39a}$$

Rearranging eqn (2.39a) and making use of eqn (2.16) which defines $k_{eff}(t)$ allows us to define $\Gamma(t)$

$$\Gamma(t) = \exp(\beta V_0)\frac{hQ}{kT}\, k_{eff}(t) . \tag{2.39b}$$

Johnston[16] has tabulated values of Γ for different values of u and α. In figure 2, $C_f(t)$ is displayed for $\alpha = 12$, and values of u of 2, 6 and 10 corresponding to tunneling corrections of 1.2, 5.2 and 162 respectively. The tunneling corrections Γ

can be obtained from the long time plateaus of $\Gamma(t)$, which are displayed in figure 3. The results can be compared to Johnston's values, and agree to the precision of his calculations.

Aside from the accuracy and economy of this calculation method, it is interesting to note the behavior of $C_f(t)$ for different u. As noted previously, the free particle correlation function has a width proportional to $\hbar\beta/2$. To be more precise, the time for it to drop to half its initial value (denoted by $t_{1/2}$) is given by $t_{1/2} = (2^{2/3}-1)^{1/2}\,\hbar\beta/2 \approx .77\hbar\beta/2$. At high temperatures where the dynamics is classically dominated we expect the half time of the correlation function for any potential to be given by the free particle value. It is interesting to see how this width changes with temperature. To this end we have calculated $C_f(t)$ for the Eckart barrier described above over a range of u from u=2 to u=400, and determined $t_{1/2}$ and $t_{1/2}/(\hbar\beta/2)$ for each calculation. These results are displayed in Table 1 where we have used units so that $u = \hbar\beta$. As expected, for the lowest u (corresponding to the highest temperature), the free particle ratio is obtained. Then as temperature decreases, the width narrows to a minimum, and finally at even lower temperatures it asymptotically approaches the free particle width again.

This behavior can be rationalized in terms of a simple uncertainty principle argument. At high temperature the Boltzmann distribution implies a large momentum distribution, so position can be localized precisely. Thus, the dynamics determining the correlation function shape are determined by the flat top of the barrier, and the result is free particle like. As temperature is lowered, the positional uncertainty increases and the dynamics probe more of the non constant part of the potential. Finally at very low temperatures the spreading due to temperature is much greater than the barrier width, so that the initial time evolution is determined by the flat asymptotic tails of the potential, leading to a free paticle like shape again.

7. *QUANTUM TRANSITION STATE THEORY IN ONE DIMENSION*

The reason that the transition state theory assumption is so useful in classical mechanics is that it is based on zero time dynamics (i.e. no dynamics). The results of the last two sections have shown that this cannot be true in quantum mechanics where the uncertainty principle broadens the correlation function about the time origin. However, the quantum $C_f(t)$ still allows us to identify "direct" dynamics on which transition state theory is conceptually based. Thus in the discussion that follows we show how this can be done by comparing the quantal and classical correlation functions for barrier problems.

To motivate our basic idea, consider the symmetrical one-dimensional Eckart barrier potential shown in figure 1. Figure 4 shows a sketch of classical and quantum flux correlation functions for a this potential, for the case that the dividing surface is chosen at the top of the barrier (s_0=0) or displaced from it ($s_0 \neq 0$). The classical flux correlation functions of figure 4 have a delta function at t=0, and it is the integral over this delta function which gives classical transition state theory, i.e.,

$$k_{CLTST} = (1/Q) \lim_{\varepsilon \to 0} \int_0^{\varepsilon} dt\, C_f^{CL}(t) \,. \tag{2.40}$$

For the case that the dividing surface is chosen at the top of the barrier (s_0=0), classical transition state theory gives the correct classical rate because there is no contribution to the time integral of $C_f(t)$ for $t > 0$. If the dividing surface is not chosen at the top of the barrier, eqn (2.40) does not give the correct rate because it omits the (negative) contribution to the integral of $C_f(t)$ for $t > 0$. (Keep in mind that the integral of $C_f(t)$ from 0 to ∞ is invariant to where the dividing surface is located, even though $C_f(t)$ itself is not.) That is, transition state theory neglects the effect of trajectories that re-cross the dividing surface, as some obviously do if the

dividing surface is not chosen at the top of the barrier. This also illustrates the variational aspect of classical transition state theory: The effect of re-crossing trajectories -- i.e., the negative lobe of $C_f(t)$ -- gives a negative contribution to the rate constant, so omitting them gives an upper bound to the rate. For transition state theory to give the best approximation to the rate one thus varies the location of the dividing surface to minimize this upper bound, i.e., to minimize the effect of re-crossing trajectories. In the present example this is accomplished quite trivially by choosing $s_0=0$.

Figure 4 also shows that quantum mechanics broadens the classical delta function at t=0 to a positive lobe of finite width (of order $\hbar\beta/2$). If the dividing surface is located at the top of the barrier, then the $C_f(t)$ has only this positive lobe, whereas it also has a negative lobe (corresponding to re- crossing flux) if the dividing surface is displaced from $s_{0=0}$. The definition of quantum mechanical transition state theory that we propose is

$$k_{QMTST} = (1/Q) \int_0^{t_0} dt\, C_f^{QM}(t) \,, \tag{2.41}$$

where t_0 is the first zero of $C_f(t)$. That is, we identify the positive lobe of the quantum $C_f(t)$ with the classical delta function at t=0, and define the quantum mechanical transition state theory rate as the area under it. It is clear that for the quantum mechanical correlation functions in figure 4 this gives an upper bound to the correct quantum mechanical rate constant because the omitted integral from $t_0 \rightarrow \infty$ gives a negative contribution. Thus, just as in the classical case, one should vary the location of the dividing surface to minimize the rate constant given by eqn (2.41).

This quantum mechanical transition state theory requires more "work" than classical transition state theory in that it is necessary to determine the dynamics,

i.e.,$C_f(t)$ for some finite amount of time, up to t_0. This is a short time, though, of order $\hbar\beta/2$. If there is no re-crossing flux--i.e., $C_f(t)$ has no negative lobe, as in figure 4 with s_0=0--then $t_0 \rightarrow \infty$, but even here $C_f(t)$ falls to zero sufficiently rapidly that as a practical matter it is still necessary to determine it only for times of order $\hbar\beta/2$. The quantum mechanical transition state theory rate is thus determined by the short time dynamics, analogous to the classical situation where it is determined by the zero time dynamics.

Consider now the unsymmetrical Eckart barrier shown in figure 5; this describes an exothermic reaction if reactants are to the left ($s \rightarrow -\infty$) and products to the right ($s \rightarrow \infty$). Figures 6a and 6b show quantum flux correlation functions like those of figure 4 for this unsymmetrical barrier. Here things look strange. With the dividing surface located at the top of the barrier (s_0=0, figure 6a) --for which there would no re-crossing effects classically--the quantum correlation function shows pronounced oscillations for $t > 0$, symptomatic of quantum re-crossing effects. If the dividing surface is moved toward reactants the oscillations are diminished [figure 6b], but in this case eqn (2.41) does not give an upper bound to the correct quantum rate constant, which violates our notion of what a transition state theory should be. Fortunately, these deficiencies are eliminated in the following way.

To see the origin of the oscillations in $C_f(t)$ for s_0=0, it is useful to recall the explicit expressions for $C_f(t)$ in a basis set (eqn (2.32))

$$C_f(t) = \sum_{i,j} \exp[-\beta(E_i+E_j)/2] \cos[(E_i-E_j)t/\hbar] \; |\langle i|F|j\rangle|^2 . \qquad (2.42)$$

The sums in eqn (2.42) are over all such eigenstates and thus include terms for which $E_i<V_r$ cf. figure 7 - i.e., whose energies are less than the asymptotic energy of reactants. The wavefunctions corresponding to these energy levels $E_i<V_r$ are non-zero predominantly on the product side of the barrier, but they do have tunneling

"tails" that are non-zero at the dividing surface $s=s_0=0$ and thus contribute to the flux there. Such states will not contribute to the net flux, though, for all the system can do at an energy less than V_r is to tunnel into the barrier region and tunnel back out; i.e., such states contribute to re-crossing flux but not any net reactive flux.

It thus seems intuitively clear that this undesired oscillatory contribution to $C_f(t)$ can be eliminated--without changing the rate constant, the integral of $C_f(t)$ --by dropping from eqn (2.42) all terms for which E_i or E_j are less than V_r. Doing so yields the correlation function in figure 6c, which has the anticipated behavior: there is now no negative lobe to $C_f(t)$ if the dividing surface is chosen at the top of the barrier. This modification of eqn (2.42) thus eliminates the "spurious" re-crossing flux in $C_f(t)$ so that eqn (2.41) once again gives a well-behaved quantum transition state theory.

To justify the above modification we note that the flux correlation function can be written in terms of any projector. So far we have chosen one that only operates on coordinate space, but now it is convenient to make a more general choice given by

$$R = h(H-V_r)\, h(s_0-s)\, h(H-V_r)\ , \tag{2.43}$$

where H is the Hamiltonian. This choice of projector requires the energy of the system to be greater than V_r, as well as requiring the system to be on the left side of the dividing surface; it is clearly an acceptable definition of the projector onto all reactant states. The symmetrical form of eqn (2.43) insures that R is hermitian. It is easy to show that the generalized flux F_r, which results from this choice of R is

$$F_r = h(H-V_r)\, F\, h(H-V_r)\ , \tag{2.44}$$

where F on the right hand side is the ordinary flux operator, eqn (2.20). Eqn (2.42) thus becomes

$$C_f(t) = \sum_{i,j} \exp[-\beta(E_i+E_j)/2] \cos[(E_i-E_j)t/\hbar] \, |\langle i|F|j\rangle|^2 h(E_i-V_r)h(E_j-V_r) \, , \qquad (2.45)$$

which is the desired result; i.e., one simply omits from the sum over states all terms for which E_i or E_j are less than V_r, and the correlation function in figure 6a becomes that in figure 6c.

The aim of this section has been to show that by identifying the direct flux from the behavior of the quantum correlation function we can approach a definition of quantum transition state theory. The major new idea introduced in order that this be feasible is that for asymmetric reactions we must project out flux from energetically forbidden processes to be able to retain our physical interpretation of the meaning of the correlation function.

8. *COMPARISON WITH OTHER CORRELATION FUNCTION EXPRESSIONS*

In section 3 of this chapter, the reactive flux correlation function was derived, and in the subsequent sections we have found this correlation function to be extremely useful in conceptualizing the ideas of transition state theory. In section 3 it was stated that the present formulation had advantages over alternate ways of defining the correlation function, for example by choosing $\lambda \neq \beta/2$ in equation 2.7, or Yamamoto's Kubo transforms-based expression.

To summarize these three expressions, which we denote as $C_f(t)$, $C_f^{\lambda}(t)$, and $C_f^{K}(t)$, respectively, we give their defining expressions below

$$C_f(t) = \mathrm{tr}\{F \exp(-\beta H/2)\, F(t) \exp(-\beta H/2)\} \, , \qquad (2.46a)$$

$$C_f^{\lambda}(t) = \mathrm{tr}\ \{\ F\exp(-\lambda H)\ F(t)\ \exp(-[\beta-\lambda]H)\ \} \, , \qquad (2.46b)$$

$$C_f^{K}(t) = \frac{1}{\beta}\int_0^{\beta} d\lambda\ \mathrm{tr}\ \{\ F\exp(-\lambda H)\ F(t)\ \exp(-[\beta-\lambda]H)\ \} \, , \qquad (2.46c)$$

where in all cases $F(t) = \exp(-iHt/\hbar)\, F \exp(iHt/\hbar)$.

Both $C_f(t)$ and $C_f^K(t)$ are real and even functions of time, while $C_f^\lambda(t)$ is complex. To show that both $C_f(t)$ and $C_f^K(t)$ are even in time we make the substitution $t \rightarrow -t$. Then cyclic permutation of the operators yields $C_f(t)$ again, while cyclic permutation and the replacement $\lambda \rightarrow \beta-\lambda$ in the integral yields $C_f^K(t)$ again. The correlation function $C_f(t)$ can be shown to be real by noting that both F and $\exp(-\beta H)$ are Hermitian operators, so

$$F^* = F$$

and

$$\exp(-\beta H)^* = \exp(-\beta H) \ .$$

Thus,

$$C_f(t)^* = C_f(-t) = C_f(t) \ .$$

The same arguement can be applied to $C_f^K(t)$ to show that it is real as well. Finally, using the same type of analysis on $C_f^\lambda(t)$, one can show that

$$C_f^\lambda(-t)^* = C_f(t) \ ,$$

which means that the real part of $C_f^\lambda(t)$ is even and the imaginary part is odd. The time dependence of each of these correlation functions is different, but the real part of the integrals from 0 to ∞ are indentical and give the rate constant.

The differences between these correlation function expressions can be illustrated by calculating values using the basis set method. We have already discussed the basis set evaluation of eqn (2.46a). The basis set expression for eqn (2.46b) is similar and yields the expression

$$C_f^{\lambda}(t) = \sum_{n\,n'} \exp(-\lambda E_n - (\beta-\lambda)E_{n'}) \cos[(E_n - E_{n'})t/\hbar] \, |\langle n|F|n'\rangle|^2 , \tag{2.47}$$

while the basis set evaluation of eqn (2.46c) is accomplished by integrating the above expression from $\lambda=0$ to $\lambda=\beta$, and is

$$C_f^{K}(t) = \sum_{n\,n'} \frac{\exp(-\beta E_n) - \exp(-\beta E_{n'})}{\beta(E_n - E_{n'})} \cos[(E_n - E_{n'})t/\hbar] \, |\langle n|F|n'\rangle|^2 . \tag{2.48}$$

Similarly, we can obtain $k_{eff}(t)$ for each of these expressions (analogous to eqn (2.34)) by integrating the expression from 0 to t. This makes the change

$$\cos[(E_n - E_{n'})t/\hbar] \rightarrow \frac{\sin[(E_n - E_{n'})t/\hbar]}{(E_n - E_{n'})/\hbar} .$$

In figures 7 and 8 we show the correlation funtions and effective rates for these three types of correlation function calculated by the basis set method. The symmetrical eckart barrier described in section 6, with u = 8, α=12 is used. This yields a tunneling correlation Γ of 22. The first correlation function in the figure is our now familiar result. For the correlation function of equation 2.46b a very nonsymmetric choice of $\lambda/\beta = 7/8$ was used. This introduces oscillatory behavior in the correlation function. Finally, unlike the first two correlation functions, the Yamamoto correlation function does not behave smoothly. Costley and Pechukas[17] have shown that the Yamamoto correlation function behaves as $|t|^{-1/2}$ around t=0, and so has an integrable singularity. Thus, its behavior cannot be exactly represented by a finite-sized discrete basis set expansion. For that case $k_{eff}(t) \simeq \frac{t}{|t|^{1/2}}$ (i.e. is nonsingular), and so may be better described by a basis set expansion. The point to note from figure 8 is that even though these correlation functions behave very differently, they all give the correct rate in a reasonably short time. (Note that all calculations used the same basis set and box size.) Considering

figure 7 again, the advantages of the symmetric choice of $C_f(t)$ are obvious. It is the only correlation function that allows us interpretation of its behavior in a physically meaninful way, which is of course what we need to do when considering transition state theory. The second correlation introduces spurious recrossings, and if a transition state rate constant were determined by the area before the first zero, it would vastly overestimate the rate (i.e. see the first peak in figure 7b).

The behavior of the Yamamoto expression merits further discussion. As discussed by Costley and Pechukas, any finite basis set evaluation of it cannot be correct near zero time, since high energy terms in eqn (2.48) are responsible for the singularity. However, the other two correlation function expressions are well behaved at the time origin. The origins of the singularity in the Yamamoto expression are the endpoints in the integral over λ. This can be inferred from the difference in behavior between figure 7a and figure 7b, but can also be shown directly by again considering the free particle correlation function expression for $\lambda \neq \beta/2$. The expression can be obtained in the same way as the symmetric λ expression was obtained in section 5, and is

$$C_f^{\lambda}(t) = \frac{kT}{h} \frac{(\hbar\beta/2)^2}{[\, t^2 + \hbar^2\lambda(\beta - \lambda) + i\hbar t(\beta - 2\lambda)]^{3/2}} \,. \tag{2.49}$$

Note that $\lambda=\beta/2$ gives the previous result. Now consider the behavior of this expression when t=0. We have

$$C_f^{\lambda}(0) = \frac{kT}{h} \frac{(\hbar\beta/2)^2}{[\, \hbar^2\lambda(\beta - \lambda)\,]^{3/2}} \,. \tag{2.50}$$

This expression is finite for all $0<\lambda<\beta$, but diverges at the endpoints of the range. Thus the Kubo expression

$$C_f^{K}(0) = \frac{kT}{h} \frac{1}{\beta} \int_0^{\beta} d\lambda \, \frac{(\hbar\beta/2)^2}{[\, \hbar^2\lambda(\beta - \lambda)\,]^{3/2}} \,, \tag{2.51}$$

has nonintegrable singularities at the endpoints of the integral going as $\lambda^{-3/2}$ as $\lambda \to 0$, and $(\beta-\lambda)^{-3/2}$ as $\lambda \to \beta$, and so is singular at the origin of time. That the singularity goes as $|t|^{-1/2}$ was shown previously[17].

We can also obtain the explicit time dependence of $C_f^K(t)$ by integrating eqn (2.49) over λ, since the integral can be done analytically[18]:

$$C_f^K(t) = \frac{1}{\beta}\int_0^\infty C_f^\lambda(t) = \frac{kT}{h}\frac{(\hbar\beta/2)^2}{[\,t^2 + \hbar^2\lambda(\beta-\lambda) + i\hbar t(\beta - 2\lambda)]^{3/2}}$$

$$= \frac{kT}{h}\,\frac{1}{2\hbar^2\beta}\left\{\frac{\hbar^2\beta+2i\hbar t}{[t^2-i\hbar t\beta]^{1/2}} + \frac{\hbar^2\beta-2i\hbar t}{[t^2+i\hbar t\beta]^{1/2}}\right\}. \tag{2.52}$$

The result is a purely real number, as it is the sum of a complex number and its complex conjugate. Eliminating the explicit imaginary terms yields the purely real expression

$$C_f^K(t) = \frac{kT}{h}\,\frac{\frac{1}{2}\left\{\frac{1}{2} + \frac{t^2/2}{[t^4+\hbar^2\beta^2t^2]^{1/2}}\right\}^{1/2} - \frac{t}{\hbar\beta}\left\{\frac{1}{2} - \frac{\hbar\beta t/2}{[t^4+\hbar^2\beta^2t^2]^{1/2}}\right\}^{1/2}}{[t^4+\hbar^2\beta^2t^2]^{1/2}}. \tag{2.53}$$

Finally, taking the limit as $t \to 0$ yields

$$C_f^K(t\approx 0) = \frac{kT}{h}\,(8\hbar\beta)^{-1/2}|t|^{-1/2}, \tag{2.54}$$

which goes as $|t|^{-1/2}$, the correct result.

Finally, consider the integral over time from 0 to ∞ of eqn (2.49). This integral is the same form as the one just done, and the result is

$$\int_0^\infty C_f^\lambda(t)\,dt = \frac{kT}{h}\left[\,1 + \frac{i\hbar(\beta/2-\lambda)}{[\hbar^2\lambda(\beta-\lambda)]^{1/2}}\,\right]. \tag{2.55}$$

Thus the real part yields the correct rate constant, while the imaginary part

disappears if $\lambda = \beta/2$.

It now seems clear why the choice $\lambda=\beta/2$ is optimal. It chooses the single value of λ farthest away from any singularity, and this choice leads to the best behaved correlation function. We note also how the idea of a Boltzmann amplitude operator as defined in section 3 (instead of a Boltzmann probability operator) makes this choice naturally, and wonder if this concept has wider applicability.

9. *SEPARABLE QUANTUM TRANSITION STATE THEORY*

Transition state theory is useful in chemistry because it yields a simple expression for the rate constant that can be easily evaluated. This expression indicates the rate in terms of the ratio of the quantum partition functions for the activated complex, and the reactant. The usual derivation of this expression involves deriving the classical expression, and then replacing the classical partition functions with quantum ones, and assuming that motion along the reaction co-ordinate can be treated classically[10].

The expression is

$$k = \frac{kT}{h}\frac{Q^{\ddagger}}{Q}\exp(-\beta V^{\ddagger}) \ . \tag{2.56}$$

However, using the reactive flux correlation function we can derive this expression correctly, and show the separable approximation explicitly. We assume that the Hamiltonian is separable in the transition state region, i.e., that

$$\begin{aligned} H &= h_s + h_Q \\ &= \frac{p_s^2}{2m} + V_0(s) + \sum_k \frac{P_k^2}{2m} + V_k(Q_k) \ , \end{aligned} \tag{2.57}$$

where s is the reaction coordinate, and where Q is a set of coordinates orthogonal to

the reaction coordinate. In this coordinate system the dividing surface is chosen to include only the s-degree of freedom, so the flux operator is a function of s and p_s only. Thus the rate can be written as

$$k = \frac{1}{Q}\int_0^\infty C_f(t)dt$$

$$= \frac{1}{Q}\int_0^\infty dt\ tr[F(s,p_s)\exp(i[h_s+h_Q]t_c/\hbar)F(s,p_s)\exp(-i[h_s+h_Q]t_c^*/\hbar)]$$

$$= \frac{1}{Q}\ tr_Q[\exp(-\beta h_Q)]\int_0^\infty dt\ tr_s[F(s,p_s)\exp(ih_s t_c/\hbar)F(s,p_s)\exp(-ih_s t_c^*/\hbar)]\ . \qquad (2.58)$$

where tr_s and tr_Q denote traces over these degrees of freedom, and the tr_Q factor is obtained since F is independent of the Q variables, and $\beta = (it_c - it_c^*)/\hbar$. The integral over time of the s dependant part gives the one dimensional rate, which can be written as a quantum correction times the classical rate (passage over the top of the barrier) i.e. $\Gamma\ \frac{kT}{h}\exp(-\beta V_0)$, while the trace over Q gives the partition function for the orthogonal degrees of freedom, typically labelled as $Q^\ddagger$. Thus the practical version of transition state theory is recovered. Of course for cases where the dynamics are not separable, this formula will can no longer be interpreted this way. However, Γ can still be defined as the ratio of the exact rate constant to the 1d separable transition state theory estimate (with classical reaction coordinate dynamics), it then includes corrections for nonseparable tunneling dynamics and dividing surface recrossing as well. The separable approximation for direct dynamics will be correct when the thermal de Broglie wavelength for motion along the reaction coordinate is short compared to changes in the Hamiltionian describing the Q degrees of freedom, and this limit is obtained at high temperatures. However, it is also at high temperatures where dividing surface recrossing is expected.

10. CONCLUSIONS

In this chapter, we have derived a general formalism that allows a new conceptual approach to the problem of chemical reaction rates. Instead of thinking of a rate in terms of transitions between asymptotic scattering states, we borrow some of the concepts of transition state theory, and define the rate in terms of quantum flux through a dividing surface. This allows us to understand quantum transition state theory in terms of direct flux identified from the reactive flux correlation functions.

Another advantage of this formalism is that it allows a more unified picture of chemical reactions. Gas phase reactions are the focus of theoretical and experimental interest because they have the hope of being treated in a completely rigorous way. However, ultimately theoretical chemistry must deal with reactions in solutions and on surfaces. The scattering theory formalism is not appropriate for such situations, while the reactive flux correlation function formalism can be readily applied to these cases, and in fact much work is being done using classical mechanics in this area[14,15]. If quantum effects are important they can be treated with the present formulation, although the basis set method described in this chapter is inappropriate. In Chapter 4 a path integral method applicable to multidimensional sysyems will be outlined that has some hope of being applied to these situations.

Chapter 3: Collinear Reactions

1. INTRODUCTION

In the previous chapter, the behavior of the reactive flux correlation function has been investigated for various one-dimensional potentials, and some correspondence with the ideas of transition state theory established. The connection between the reactive flux correlation function, and the typical version of separable quantum transition state theory has also been established. However, one of the drawbacks of the use of separable transition state theory is that the transition state dynamics are typically not separable, so inaccurate results can be obtained even if the assumptions of transition state theory are valid[19]. This effect cannot be investigated in one-dimensional systems, and so a two- dimensional model must be considered. In this chapter, we study three reactions of the type

$$A + BC \rightarrow AB + C$$

where all the atoms are constrained to lie on the same line. Elimination of centre of mass motion reduces this to a two-dimensional problem. The collinear problem is the simplest system that can be considered a realistic model for a chemically reacting system. Different regions on the potential surface can be identified as reactant and product, consisting of one internal degree of freedom (the BC or AB stretch), and a translational degree of freedom that brings the reacting fragments closer together or farther apart. Also, in the interaction region (the region where A,B, and C are all close together) the reaction co-ordinate can be strongly coupled to the other degree of freedom. In a reaction path Hamiltonian picture[20] , this

coupling can take two forms: curvature of the reaction path, and variation of the frequency of the degree of freedom orthogonal to the reaction path along the reaction path.

Thus, in this chapter calculations of the quantum reactive flux correlation function for three different collinear atom-diatom reactions over a range of temperatures will be described. The three systems studied are the $H + H_2$ reaction on the Porter-Karplus surface[21,22,23], the Cl + HCl reaction on a LEPS surface[24], and the $F + H_2$ reaction on the Muckerman-5 surface[25,26,27]. The purpose of this chapter is to illustrate the generic behavior of the quantum correlation function for different kinds of reaction dynamics. We also calculate the classical reactive flux correlation functions for the same potential surfaces. This allows us to interpret features in the quantum correlation function in terms of classical features that can be explained in terms of individual trajectories.

2. *THEORY AND METHOD*

a. Quantum Calculations

For the quantum calculations we use the basis set method that was described in the previous chapter. However, the work in the present chapter deals with a two-degree-of-freedom system, demanding the use of a different basis set. The next part of the chapter contains a description of the Hamiltonian for the system and of the basis set used, as well as some of the details of the calculation of the Hamiltonian and flux operator matrix elements.

For these calculations we have found it convenient to work in hyperspherical (i.e. polar) co-ordinates. There are several reasons for this choice. First of all, it is well known that for collinear systems the Hamiltonian in terms of r_{AB} and r_{BC} contains cross terms between these co-ordinates in the kinetic energy operator. The kinetic energy can be easily made diagonal by making a co-ordinate change

(described below) that leads to the skewed co-ordinate system[28].

Now we need a basis set that confines the system to the interaction region in the potential. This is most easily done in terms of polar co-ordinates, by confining the system to $\rho=\rho_{max}$ by placing a wall at ρ_{max}. Finally, previous work has shown that the vibrationally adiabatic approximation works well in hyperspherical co-ordinates[29,30], and the basis set we use will be based on this.

In hyperspherical coordinates, the Hamiltonian is given by

$$H = -\frac{\hbar^2}{2\mu}\left(\frac{1}{\rho}\frac{\partial}{\partial\rho}\rho\frac{\partial}{\partial\rho} + \frac{1}{\rho^2}\frac{\partial^2}{\partial\theta^2}\right) + V(\rho,\theta) , \tag{3.1}$$

where the reduced mass μ is defined in terms of the masses of the three particles by

$$\mu = \left(\frac{m_A m_B m_C}{m_A + m_B + m_C}\right)^{1/2} . \tag{3.2}$$

The coordinates ρ and θ can be related to r_{AB} and r_{BC} in the following way:

$$x = \rho \cos(\theta) ,$$

$$y = \rho \sin(\theta) ,$$

$$r_{AB} = x/A - m_C A y/(m_B+m_C) ,$$

$$r_{BC} = Ay , \tag{3.3}$$

where $A = [m_A(m_B+m_C)^2/(m_B m_C(m_A+m_B+m_C))]^{1/4}$.

The coordinate ρ varies from zero to infinity, with $\rho = 0$ corresponding to the three particle coincidence, and $\rho = \infty$ corresponding to the particles being infinitely separated. The coordinate θ ranges from $\theta = 0$ to $\theta = \theta_m$ the skew angle defined in terms of the masses by

$$\theta_m = \tan^{-1}[\frac{m_A(m_A+m_B+m_C)}{m_A m_C}]^{1/2} . \tag{3.4}$$

The potential surfaces are defined in terms of r_{AB} and r_{BC}.

The vibrationally adiabatic approximation works well for collinear systems in hyperspherical coordinates, when θ is treated as the fast coordinate, and ρ as the slow coordinate. Thus, in the present work we chose a vibrationally adiabatic basis set:

$$\phi_{mn}(\rho,\theta) = \rho^{-1/2}\, \chi_n(\rho)\, f_m(\theta;\rho) . \tag{3.5}$$

The radial basis function $\chi_n(\rho)$ is defined as a particle in a box function:

$$\chi_n(\rho) = [\frac{2}{L}]^{1/2} \sin[n\pi\frac{\rho-\rho_{min}}{L}] , \tag{3.6}$$

where $L = \rho_{max}-\rho_{min}$, and ρ_{min} and ρ_{max} are chosen to be small enough and large enough respectively that the walls do not interfere with the dynamics over the time scale that the correlation function is nonzero. The vibrational basis functions $f_m(\theta;\rho)$ depend parametrically on ρ, and are obtained by numerically solving the one dimensional Schrodinger equation[31] that results upon fixing ρ

$$[\frac{-\hbar^2}{2\mu}\frac{1}{\rho^2}\frac{\partial^2}{\partial\theta^2} + V(\rho,\theta) - E_m(\rho)]\, f_m(\theta;\rho) = 0 . \tag{3.7}$$

We now obtain matrix elements of the Hamiltonian in this basis set, by first operating on a basis function to the right with the Hamiltonian to obtain

$$H\,\phi_{mn}(\rho,\theta) = \rho^{-1/2}\{\frac{-\hbar^2}{2\mu}[f_m(\theta;\rho)\frac{\partial^2}{\partial\rho^2}\chi_n(\rho) + 2(\frac{\partial}{\partial\rho}f_m(\theta;\rho))(\frac{\partial}{\partial\rho}\chi_n(\rho))$$

$$+ \chi_n(\rho)\frac{\partial^2}{\partial\rho^2}f_m(\theta;\rho)] + [E_m(\rho) - \frac{\hbar^2}{8\mu\rho^2}]\}\chi_n(\rho)f_m(\theta;\rho)\ . \tag{3.8}$$

Now we operate from the left with a different basis function, and perform the integrals over θ and ρ to obtain

$$\langle n'm'|H|nm\rangle = -\frac{\hbar^2}{2\mu}(\frac{n\pi}{L})^2\,\delta_{mm'}\,\delta_{nn'}$$

$$+ 2\int d\rho\chi_{n'}(\rho)\,[\frac{\partial}{\partial\rho}\chi_n(\rho)]\,c^{(1)}_{mm'}(\rho)$$

$$+ \int d\rho\,\chi_{n'}(\rho)\,\chi_n[c^{(2)}_{mm'}(\rho) + \{E_m(\rho) - \frac{\hbar^2}{8\mu\rho^2}\}]\ , \tag{3.9}$$

where the new coupling functions are defined by

$$c^{(1)}_{mm'}(\rho) = \int d\theta\ f_{m'}(\theta;\rho)\frac{\partial}{\partial\rho}f_m(\theta;\rho)\ , \tag{3.10a}$$

$$c^{(2)}_{mm'}(\rho) = \int d\theta\ f_{m'}(\theta;\rho)\frac{\partial^2}{\partial\rho^2}f_m(\theta;\rho)\ . \tag{3.10b}$$

These terms correspond to non-adiabatic couplings which are an important contribution whenever the vibrationally adiabatic approximation breaks down. In our calculations they are computed by finite differences over the same grid as the numerical integrals over ρ.

The Hamiltonian can then be diagonalized to produce eigenvalues $\{E_k\}$ and eigenvectors $\{U_{mn,k}\}$. The flux correlation function is given by the familiar expression

$$C_f(t) = \sum_k \sum_{k'} \exp[-\beta(E_k + E_{k'})/2]\cos[(E_k - E_{k'}t/\hbar]\,|\langle k|F|k'\rangle|^2 . \tag{3.11}$$

For symmetric reactions the matrix elements of the flux operator are given by

$$\langle k|F|k'\rangle = \sum_{nm} \sum_{n'm'} U_{n'm',k'} \langle n'm'|F|nm\rangle U_{nm,k} , \tag{3.12}$$

since, for these reactions the dividing surface is a straight line through the symmetry axis and it is convenient to obtain matrix elements of the flux operator directly in the basis set:

$$\langle n'm'|F|nm\rangle = \frac{\hbar}{2m} \int d\rho\, \chi_n(\rho)\chi_{n'}(\rho)$$

$$\{[\frac{\partial f_{m'}(\theta;\rho)}{\partial\theta}|_{\theta=\theta_D}]\, f_m(\theta_D;\rho) - f_{m'}(\theta_D;\rho)[\frac{\partial f_m(\theta;\rho)}{\partial\theta}|_{\theta=\theta_D}]\} , \tag{3.13}$$

where $\theta_D = \theta_m/2$, half the skew angle. For the $F + H_2$ reaction there is no symmetrically defined dividing surface, so we take the dividing surface to be defined by

$$\theta_D(\rho) = 1/2\theta_d\{1 + \tanh[(\rho - \rho_0)/\Delta\rho]\} , \tag{3.14}$$

where the parameters θ_d , ρ_0 , and $\Delta\rho$ are chosen so that the dividing surface coincides to the variational transition state theory dividing surface. Matrix elements of the step function are obtained in the basis set

$$\langle n'm'|h(\theta - \theta_D(\rho)|nm\rangle = \int d\rho\, \chi_n(\rho)\, \chi_{n'}(\rho) \int_{\theta_D(\rho)}^{\theta_m} d\theta\, f_m(\theta;\rho)\, f_{m'}(\theta;\rho) , \tag{3.15}$$

and transformed to the eigenstate basis as in eqn (3.12). Then the eigenstate basis matrix element is given by

$$<k|F|k'> = <k|\frac{i}{\hbar}[H,h(\theta-\theta_D(\rho))]|k'> \tag{3.16}$$

$$= \frac{i}{\hbar}(E_k - E_{k'})<k|h(\theta-\theta_D(\rho))|k'> .$$

b. Classical Calculations

We wish to compare the quantum correlation functions with classical correlation functions to determine which of the features observed have a classical explanation, and which are quantum effects. The first problem that arises in this comparison is the fact that the true classical correlation function has a delta function at the origin, the size of which is given by classical transition state theory (see discussion in Chapter 2, section 4). The quantum correlation function is spread out by the uncertainty principle, and instead has a width of about $\hbar\beta/2$.

To minimize this well understood difference between the classical and quantum correlation functions we have therefore chosen to "smear out" the classical delta function by averaging the classical correlation function over a time interval of order $\hbar\beta/2$. Specifically, we define the quasi-classical expression according to

$$C_f^{QCL}(t) = \frac{2}{\hbar\beta\sqrt{\pi}} \int_{-\infty}^{\infty} dt' \exp[-(t-t')^2/(\hbar\beta/2)^2] C_f^{CL}(t') , \tag{3.17}$$

where $C_f^{CL}(t)$ was defined in eqn (2.22). The primary effect of this averaging is to replace the delta function in the classical correlation function by a peak whose width is about $\hbar\beta/2$.

Another source of disagreement of the purely classical correlation function from its quantum counter part is the quantization of the "activated complex"; eg. within the short time approximation $Q^{\ddagger}$ is a quantum vibrational partition function in the quantum case, and a classical one for the classical case, and these can differ substantially in their numerical values. To patch up this defect we have used the

often-applied quasi-classical model. Thus the initial values (P_1,Q_1) are specified in terms of the action-angle variables for this degree of freedom. For a harmonic oscillator, for example,

$$Q_1 = \left(\frac{(2n_1 + 1)\hbar}{m\omega}\right)^{1/2} \sin q_1 \ , \tag{3.18a}$$

$$P_1 = ((2n_1 + 1)\hbar m\omega)^{1/2} \cos q_1 \ . \tag{3.18b}$$

(In the applications presented herein the Q–oscillator is taken to be a Morse oscillator, for which equation analogous to eqn (3.18) are more complicated, but still known.[32]) The $(P_1,Q_1) \longleftrightarrow (n_1,q_1)$ transformation is canonical, so an integral over P_1 and Q_1 is identical to an integral over n_1 and q_1 , but the quasi-classical model is to sum over integer values of n_1; thus eqn (2.22) for $C_f^{CL}(t)$ is modified as follows,

$$(2\pi\hbar)^{-1} \int dP_1 \int dQ_1 \rightarrow \sum_{n_1=0} (2\pi)^{-1} \int_0^{2\pi} dq_1 \ . \tag{3.19}$$

(It should be noted that this same type of quasi-classical initial condition for the activated complex has also been used for full classical trajectory calculations for reactive scattering[33]/.) For the temperature range of our calculations, essentially only the $n_1=0$ -i.e. the ground state of the activated complex - contributes signifigantly. Also, by definition of the action angle variables, one has

$$\frac{P_1^2}{2m} + V(s_0,Q_1) = \varepsilon_{n_1} \ , \tag{3.20}$$

where ε_{n_1} is the vibrational energy level of the activated complex.

In summary, then, with the modifications implied by eqns (3.17) - (3.20), and with the choice $s_0=0$, the quasi-classical expression for the reactive flux correlation function is

$$C_f^{QCL}(t) = \sum_{n_1=0} \exp(-\beta\varepsilon_{n_1})\,(2\pi)^{-1} \int_0^{2\pi} dq_1 \int_{-\infty}^{\infty} dp_1 \exp(-\beta\frac{p_1^2}{2m})\,(p_1/m)$$

$$\frac{2}{\hbar\beta\sqrt{\pi}} \sum_k \text{sign}\,[p(t_k)]\,\exp[-(t-t_k)^2/(\hbar\beta/2)^2]\,, \tag{3.21}$$

where s(t) and p(t) are the classical trajectories determined by the initial conditions $(n_1, q_1, p_1, s_1=0)$, and $\{t_k\}$ are the times for which s(t)=0.

3. *RESULTS*

In this section we compare the quantum and classical correlation functions for the three reactions to see to what extant the various dynamical features observed in the quantum correlation functions can be understood classically. To this end we display the correlation functions all normalized to their value at t=0; i.e. the quantities plotted are $C_f(t)/C_f(0)$. We note that the integrals of the quantum correlation functions yield the correct quantum rate constants in all cases.

Table 2 gives various quantities which characterize the quantum correlation functions, and also gives (in the last column) the ratio of the correct quantum rate to the non-tunnelling, conventional transition state theory rate (with quantum $Q^{\ddagger}$). This ratio is the historical[1] " κ " which corrects all the defects of conventional transition state theory (i.e. neglect of tunnelling and re-crossing).

a. $H + H_2 \rightarrow H_2 + H$

This is the simplest known chemical reaction, and it has been studied extensively. In classical mechanics it is known that microcanonical transition state theory is exact for energies up to approximately 0.4 eV above the reaction threshold[34]. Since the thermal energy at 1000 K, the highest temperature considered, is only 0.09 eV, one would not expect to see any effects of recrossing dynamics. That this is true can be seen by noting that none of the $H+H_2$ correlation functions, quantum or classical, displayed in figures 9 and 10 are ever negative; i.e. all reactive dynamics is "direct".

The differences between the classical and quantum correlation functions in figures 9 and 10 are therefore due solely to tunnelling effects. To quantify the discussion somewhat, we define $t_{1/2}$ as the time at which $C_f(t)$ has fallen to half its value at t=0. If the behavior is free particle-like - as all of the classical correlation functions are for short times because of the averaging done by eqn (3.17) - then this half time would be $(2^{2/3}-1)^{1/2}\hbar\beta/2 = .77(\hbar\beta/2)$. Free particle, non-tunnelling short time behavior is characterized by the ratio $t_{1/2}/(\hbar\beta/2) = 0.77$. Table 2 lists these values for all the reactions.

At the highest temperature, 1000 K, the effect of tunnelling is small (κ=1.5), and the half time for the decay or the quantum correlation function is essentially the classical value. (cf. Table 2a). The half-time increases with decreasing temperature, but not as fast as $\hbar\beta$, and appears to be reaching a limit; i.e. the width of $C_f(t)$ in figure 9 is essentially the same for T=200 K and T=300 K. This can be understood because the reaction is dominated by tunnelling at T=200 K (κ=46), and it has been shown previously[8] that the correlation function for a parabolic barrier, the generic tunnelling system, decays as $\exp(-2\omega_b t)$, where ω_b is the imaginary frequency of the barrier; i.e. the decay is temperature independent when tunnelling dominates. For

this system ω_b = 200 au, which is seen to be the order of magnitude observed for the decay of $C_f(t)$ in the low temperature limit.

One notes therefore, that when tunnelling effects dominate, the time averaging of the classical correlation function, eqn (3.17), does not describe the quantum short time dependence correctly.

b. Cl + HCl → ClH + Cl

The Cl + HCl example is a typical example of a heavy-light-heavy system where a small mass is transferred between two large ones. The quantum and classical correlation functions for this system are shown in figures 11 and 12. Classically such a system can exhibit multiple recrossings, since motion through the dividing surface is in the same direction as vibrational motion of the reactants and products. Quantum mechanically such recrossing is indeed observed at higher temperatures.

First consider the quantum correlation function at T=200 K. It shows almost no recrossing so that any discrepancy between conventional transition state theory and the exact quantum rate must be due to tunneling. From Table 2b one sees that there is indeed signifigant tunneling at T=200 K.

As temperature increases, the recrossing becomes much more pronounced, and the importance of tunneling decreases. Thus the transition state theory rate - which omits the effects of recrossing - begins to overestimate the rate constant; cf. the last column in Table 2b. For a system such as Cl+HCl with a high skew angle the best classical variational dividing surface occurs at the symmetric location only for low energies. Above a certain critical energy, the symmetric periodic orbit dividing surface surface becomes unstable and bifurcates into two symmetrically equivalent dividing surfaces[35,36]. From the point of view of transition state theory, it is clear that a better short time estimate of the rate constant can be obtained by moving the

dividing surface to the variational location. However, since we are interested in obtaining the exact rate in the shortest possible time, it is more advantageous to place the dividing surface in the symmetric location. It is clear that this should give the quickest convergence, since the rate is determined by the dynamics through both bottlenecks, and the symmetric location treats them equivalently. We note also that the classical correlation function accurately mimics the oscillatory features of the quantum function at temperatures where recrossing occurs.

c. $F + H_2 \rightarrow FH + H$

Finally we consider a more realistic example of a chemical reaction. This potential is no longer symmetric, so chemical change occurs during the reaction. The FH molecule is much more strongly bound than the H_2 molecule, and so $F + H_2$ (v=0) can react at thermal energies to produce products in any of the four lowest states of FH. The probabilities of forming HF (v=0) and HF (v=1) are almost negligible, but HF (v=2) and HF (v=3) are both produced at thermal energies[26].

The quantum and classical correlation functions for this system are displayed in figures 13 and 14, and the half-times for the decay of the correlation functions and the comparison to transition state theory are shown in Table 2c. We note at this point that in order to obtain the quantum results shown, it was necessary to change the definition of the flux operator as discussed in Chapter 2 section 7 so that states that lack sufficient energy to exist asymptotically as reactants are not included in the trace. The only change from a computational point of view is that in eqn (3.11) the sum is restricted to eigenvalues with energies greater than the zero point energy of H_2.

Note first in figures 13 and 14 (and from Table 2c) that the short time decay of the quantum and classical correlation functions is essentially the same, indicating

that tunneling has a minor effect for this reaction. This is expected, of course, because the barrier is quite low and flat. The next most obvious feature is that there are significant re-crossing effects in the correlataion functions at all temperatures, both quantally and classically. At low enough temperature one knows that transition state theory must become exact classically[6], so that re-crossing effects must disappear; it is apparent in this case that 200 K is not yet low enough.

Though the classical re-crossing effects seen in figure 14 are in rough agreement with the quantum behavior in figure 13, there are differences: the quantum correlation function appears to oscillate about the classical value. This is most apparent at T = 1000 K, though also recognizable at other temperatures, and the spacing between minima is $\Delta t \sim 500$ au. This behavior can be understood by noting that there is a scattering resonance, i.e., a short-lived collision complex, for this system at a collision energy of 0.015 ev[37]. The Boltzmann population will thus access this resonance at all the temperatures considered here. Since the dividing surface in this case is in the entrance valley, the part of the collision complex that breaks-up non-reactively will re-cross the dividing surface on its way back to reactants. This will lead to negative contributions to $C_f(t)$ spaced by time intervals that roughly correspond to the vibrational period of the classical motion of the collision complex. I.e., the complex can break-up non-reactively, with various probabilities, after one oscillation in the complex, after two oscillations in the complex, etc.; cf. the semiclassical description of this by Waite and Miller[38]. One thus identifies the spacing Δt with $2\pi/\omega$, where ω is the vibrational frequency of the collision complex. The observed value $\Delta t \sim 500$ au gives $\omega \sim 2800$ cm^{-1}, a sensible value.

4. CONCLUDING REMARKS

The reactive flux correlation function is a useful way to characterize chemical reaction rates since it bridges the gap between transition state theory (through its short time behavior) and the dynamically exact rate constant. This chapter has considered three different A + BC reactions to illustrate the way various dynamical phenomena are manifest in this correlation function.

H + H_2 shows the simplest, transition state theory-like dynamics, its only complicating factor being quantum tunneling at the lower temperatures. Cl + HCl shows transition state theory - violating dynamics, i.e., re-crossing flux, but this is well-described within classical mechanics. Finally, F + H_2 shows non-classical re-crossing effects that one can identify with the formation of a short-lived collision complex, i.e., a scattering resonance.

These results show clearly the range of utility of the transition state idea. In the reactions where the dynamics is direct, the correlation function decays to zero quickly and the transition state theory rate estimated from its behavior is correct. In more complicated reactions, the dynamics must be followed for times long enough for the reacting system to decide on its reactive or nonreactive nature. For systems where complex formation occurs this time can be very much longer than the direct reaction time.

Chapter 4: Path Integral Calculation of the Reactive Flux Correlation Function for Systems with Many Degrees of Freedom

1. INTRODUCTION

As has been emphasized throughout this thesis, the reactive flux correlation function can be used as a bridge between the exact rate constant and attempts at the definition of a quantum transition state theory. The previous two chapters have taken the approach of examining the detailed behavior of the correlation function for some systems where it can be calculated exactly using the basis set approach. This method will not be useful for systems with many degrees of freedom

Thus, in this chapter we describe a method of calculation that has the advantage over basis set methods in that it is not limited to small dimensionality systems. This method is based upon the numerical evaluation of a discretized version of the Feynman path integral expression for the complex time propagator that occurs in a co-ordinate representation of the reaction flux correlation function. The integral over all possible Feynman paths is done by a Monte Carlo procedure, the convergence of which requires that the integrand be a positive definite quantity. This is achieved by making the substitution $\tau = it$ and performing the calculation over the range $-\hbar\beta/2 < \tau < \hbar\beta/2$.

However, the rate constant is obtained by taking the integral of the correlation function over real values of time. We give up on the goal of being able to obtain $C_f(t)$ for all times, and obtain it out to $t = \hbar\beta$ by analytic continuation of a function fit to the imaginary time values. This approach is thus similar in spirit to our previous definition of quantum transition state theory as the area under the first positive lobe

of $C_f(t)$, but implements it in a practical (although approximate) fashion. In principle this approach can be extended to arbitrary multidimensional potentials, since the success of Monte Carlo integration does not depend on the dimensionality of the resultant integral. However, for reasons that are not well understood, this approach never seemed to work. An approach that was successful, and that will be described in the following sections, was to approximate the multidimensional nature of the problem as a reaction co-ordinate coupled to a multidimensional variable frequency harmonic bath with reaction co-ordinate dependent coupling. A numerical method can be developed to do the path integral over these degrees of freedom exactly, yielding a one dimensional path integral calculation in terms of an influence functional.

This work is related to other work done by Jacquet and Miller[39], and Yamashita and Miller[40]. The major advances introduced here are the form of the Hamiltonian, the exact calculation of the influence functional, and the analytic continuation procedure.

In section 2 of the chapter, a complete description of the path integral calculation, and potential approximation will be provided with an analysis of the restrictions inherent in the potential approximation. The analytic continuation method is also discussed. The methodology is applied to the collinear $H + H_2$ reaction in section 3, where its accuracy can be determined by comparison to the basis set calculations. Finally in section 4 the applicability of this method to different systems is discussed.

2. *THEORY AND COMPUTATIONAL METHOD*

a. Path Integral Expression for the Flux Correlation Function

It is convenient to evaluate the reactive flux correlation function in the coordinate representation since the coordinate representation matrix elements of the imaginary time propagator can be obtained by Feynman path integration. For a symmetric potential the expression is a multidimensional generalization of eqn (2.28)

$$C_f(t) = \int dQ \int dQ' \frac{\partial^2}{\partial s \partial s'} \, |\langle s\, Q | \exp[-(\beta/2 + it/\hbar)\, H] | s' Q' \rangle|^2 , \tag{4.1}$$

with $s=s'=0$, and where s is the reaction coordinate, **Q** are the orthogonal degrees of freedom, and the dividing surface is located at s=0, and is independent of **Q**.

Straight forward Monte Carlo evaluation of the path integral representation of eqn (4.1) is not feasible because the complex exponential makes the integrand oscillatory. We thus make the substitution $\tau = it$, and evaluate eqn (4.1) for values of τ between $-\hbar\beta/2$ and $\hbar\beta/2$. This yields a positive definite integrand which can be evaluated by a Monte Carlo procedure described below. To obtain values of $C_f(t)$ for real times, we fit the values of $C_f(\tau)$ to a function based on the known analytic form of the free particle correlation function. Making this replacement to eqn (4.1) yields

$$C_f(\tau) = (\hbar/2m)^2 \frac{\partial^2}{\partial s_0 \partial s_n} \int dQ_0 \int dQ_n$$

$$\langle s_0\, Q_0 | \exp[-(\beta/2 - \tau/\hbar)\, H] \, | s_n Q_n \rangle$$

$$\langle s_n\, Q_n | \exp[-(\beta/2 + \tau/\hbar)\, H] \, | s_0 Q_0 \rangle \,, \tag{4.2}$$

with $s_0 = s_n = 0$ after differentiation.

As will be shown in later discussion, the multidimensional nature of these coordinate representations of the Boltzmann operator will be included through an influence functional, yielding an effective one dimensional path integral expression Thus consider first the Feynman path integral expression for a one-dimensional Hamiltonian of the form

$$H = \frac{p^2}{2m} + V(x) \tag{4.3}$$

for co-ordinate matrix elements of the Boltzmann operator:

$$\langle x_N | \exp(-\beta H) | x_0 \rangle = \int_{-\infty}^{\infty} dx_1 \int_{-\infty}^{\infty} dx_2 \cdots \int_{-\infty}^{\infty} dx_{N-1} \left(\frac{Nm}{2\pi\hbar^2\beta}\right)^{N/2}$$

$$\exp\left[\frac{-mN}{2\hbar^2\beta} \sum_{i=1}^{N} (x_i - x_{i-1})^2 - \frac{\beta}{N} \sum_{i=1}^{N} V\left(\frac{x_i + x_{i-1}}{2}\right)\right] . \tag{4.4}$$

We want to perform this integral by Monte Carlo, and so the question is how to choose the points in path space to sample over. For this expression it is convenient to make use of the fact that the kinetic energy part of the expression leads to Gaussian integrals which can be done. First we introduce the notation

$$I = \langle x_N | \exp(-\beta H) | x_0 \rangle$$

$$= \int_{-\infty}^{\infty} dx_1 \cdots \int_{-\infty}^{\infty} dx_{N-1} W(x_1 \cdots x_{N-1}) f(x_1 \cdots x_{N-1}) \ . \tag{4.5}$$

where W(x) corresponds to the kinetic energy part, and f(x) to the potential part (or influence functional in the multidimensional case). We want to rewrite the integral in terms of new integration variables w which range between zero and one (for convenience in generating random variables for Monte Carlo integration). For efficiency, we want all sampled points to be equally important, i.e. we want to be able to write

$$I = C \int_0^1 dw_1 \int_0^1 dw_2 \cdots \int_0^1 dw_{N-1} f(\mathbf{x}(\mathbf{w})) \ , \tag{4.6}$$

where $\mathbf{x}(\mathbf{w})$ and the normalization constant C are to be determined. If we do this, then a new path can be sampled by generating N-1 random numbers between 0 and 1 corresponding to each integral variable. The constant C is easy to determine by considering the case where f(x)=1. Comparing eqns (4.5) and (4.6) immediately yields

$$C = \int_{-\infty}^{\infty} dx_1 \int_{-\infty}^{\infty} \cdots dx_{N-1} W(x_1 \cdots x_{N-1}) \ . \tag{4.7}$$

This integral can easily be done following the procedure outlined by Feynman[41] and yields the free particle propagator, as it must if f=1 (V=0), so explicitly we have

$$C = \left(\frac{m}{2\pi\hbar^2\beta}\right)^{1/2} \exp\left[\frac{-m}{2\hbar^2\beta}(x_N - x_0)^2\right] \ . \tag{4.8}$$

Determining the co-ordinate transformation is more involved. It can be done by defining the notation

$$W_{N-1}(x_1 \cdots x_{N-1}) = W(x_1 \cdots x_{N-1}) \,, \tag{4.9}$$

where the unsubscripted W was defined previously, and denoting the rest of a series of functions $\{W_i\}$, $i = 1,\ldots,N-1$, where each function depends only on the variables $\{x_k\}$, $k = 1,\ldots,i$. Then we can write the identity

$$W_{N-1}(x_1 \cdots x_{N-1}) = \frac{W_{N-1}(x_1 \cdots x_{N-1})}{W_{N-2}(x_1 \cdots x_{N-2})} \cdot \frac{W_{N-2}(x_1 \cdots x_{N-2})}{W_{N-3}(x_1 \cdots x_{N-3})} \cdots \frac{W_1(x_1)}{W_0} \cdot W_0 \,. \tag{4.10}$$

Keeping track of the variables that W_i depends on allows us to write

$$I = W_0 \int_{-\infty}^{\infty} \frac{W_1}{W_0} dx_1 \int_{-\infty}^{\infty} \frac{W_2}{W_1} dx_2 \cdots \int_{-\infty}^{\infty} \frac{W_{N-1}}{W_{N-2}} f(x_1 \cdots x_{N-1}) \,. \tag{4.11}$$

Comparing eqn (4.11) with eqn (4.6), we make the identification

$$w_k = \int_0^{w_k} dw_k' = \int_{-\infty}^{x_k} \frac{W_k(x_1 \cdots x_k')}{W_{k-1}(x_1 \cdots x_{k-1})} dx_k' \,. \tag{4.12}$$

Now when $w_k = 1$, $x_k = \infty$, so we immediately obtain the definition of W_{k-1} in terms of W_k:

$$W_{k-1}(x_1 \cdots x_{k-1}) = \int_{-\infty}^{\infty} dx_k W_k(x_1 \cdots x_k) \,. \tag{4.13}$$

Thus, we can write the expression for w_k in explicit form where we use the notation $\Delta\tau = \hbar\beta/N$ (as before)

$$w_k = \frac{\int_{-\infty}^{x_k} dx_k' \cdots \int_{-\infty}^{\infty} dx_{N-1}' \exp[\frac{-m}{2\hbar\Delta\tau} \sum_{i=1}^{N} (x_i' - x_{i-1}')^2]}{\int_{-\infty}^{\infty} dx_k' \cdots \int_{-\infty}^{\infty} dx_{N-1}' \exp[\frac{-m}{2\hbar\Delta\tau} \sum_{i=1}^{N} (x_i' - x_{i-1}')^2]} \,. \tag{4.14}$$

All of the integrals in the denominator can be done, and all in the numerator except the one over x_k' by the procedure described by Feynman[41] since they are Gaussian integrals. Finally, making a change of variables for the last integration variable x_k as

$$z_k = [\frac{m}{2\pi\hbar\Delta\tau}\frac{(N-k+1)}{(N-k)}]^{1/2}[x_k - \frac{x_N + (N-k)x_{k-1}}{(N-k+1)}] , \tag{4.15}$$

allows us to write

$$w_k = \int_{-\infty}^{z_k} dz \exp(-\pi z^2) . \tag{4.16}$$

Formally inverting this finally yields the expression for x_k:

$$x_k = \frac{(N-k)x_{k-1}}{N-k+1} + \frac{x_N}{N-k+1} + [\frac{2\pi\hbar\Delta\tau}{m}\frac{(N-k)}{(N-k+1)}]^{1/2} z(w_k) , \tag{4.17}$$

where z(w) is the inverse of w(z), the error function defined above. While there is no analytic expression for z(w), accurate rational approximations exist[42], so it can be considered a known function for computational purposes.

We have just demonstrated how to generate random paths in the one dimensional Feynman path integral expression for the imaginary time propogator. We now show how this methodology can lead to an expression for the imaginary time reactive flux correlation function that can be directly evaluated by Monte Carlo. The two Boltzmann operators in the eqn (4.2) are written as a discretized Feynman path integral where the same imaginary time increment $\Delta\tau = \hbar\beta/N$ is used in both path integrals. For this to be true, τ must be chosen as one of the values τ_n

$$\tau_n = \hbar\beta(\frac{n}{N} - \frac{1}{2}) ,$$

$$n = 1 , \ldots , N-1 . \tag{4.18}$$

This leads to the following expression for the correlation function

$$C_f(\tau) = (\frac{\hbar}{2m})^2 \frac{\partial^2}{\partial s_0 \partial s_n} (\frac{mN}{2\pi\hbar^2\beta})^{N/2}$$

$$\int ds_1 \cdots \int ds_{n-1} \int ds_{n+1} \cdots \int ds_{N-1} \int dQ_0 \cdots \int dQ_{N-1}$$

$$\exp[-\frac{mN}{2\hbar^2\beta} \sum_{i=1}^{N} (s_i - s_{i-1})^2 - \frac{mN}{2\hbar^2\beta} \sum_{i=1}^{N} |Q_i - Q_{i-1}|^2$$

$$-\frac{\beta}{N} \sum_{i=1}^{N} V(\frac{s_i + s_{i-1}}{2}, \frac{Q_i + Q_{i-1}}{2})] . \tag{4.19}$$

where $Q_N = Q_0$ and F-1 is the number of Q degrees of freedom. It is useful to define the partition functional for the Q degrees of freedom,

$$Z_Q[s(\tau)] = [(\frac{mN}{2\pi\hbar^2\beta})^{N/2}]^{F-1} \int dQ_0 \cdots \int dQ_{N-1}$$

$$\exp[-\frac{mN}{2\pi\hbar^2\beta} \sum_{i=1}^{N} |Q_i - Q_{i-1}|^2 - \frac{\beta}{N} \sum_{i=1}^{N} V(\frac{s_i + s_{i-1}}{2}, \frac{Q_i + Q_{i-1}}{2})] , \tag{4.20}$$

which allows the correlation function expression to be written as

$$C_f(\tau) = (\frac{\hbar}{2m})^2 \frac{\partial^2}{\partial s_0 \partial s_n} (\frac{mN}{2\pi\hbar^2\beta})^{NF/2}$$

$$\int ds_1 \cdots \int ds_{n-1} \int ds_{n+1} \cdots \int ds_{N-1}$$

$$\exp[-\frac{mN}{2\hbar^2\beta} \sum_{i=1}^{N} (s_i - s_{i-1})^2] Z_Q[s(\tau)] \ . \tag{4.21}$$

In the next section of the chapter we describe how to obtain the partition functional $Z_Q[s(\tau)]$ for an arbitrary path $s(\tau)$ in the potential approximation that we introduce.

The correlation function expression that we desire can be obtained immediately from eqn (4.21) by applying the random walk procedure described above twice, once for the path from $s_1 \rightarrow s_{n-1}$, and again for the path from $s_{n+1} \rightarrow s_{N-1}$. This yields the explicit result

$$C_f(\tau_n) = (\hbar/2m)^2 \frac{m}{2\pi\hbar((\hbar\beta/2)^2 - \tau_n^2)^{1/2}} \frac{\partial^2}{\partial s_0 \partial s_n} f(s_0, s_n) \ , \tag{4.22}$$

with

$$f(s_0, s_n) = \exp[-\frac{m\beta}{2} \frac{(s_n - s_0)^2}{(\hbar\beta/2)^2 - \tau_n^2}] \int_0^1 dw \ Z_Q[s(\tau)] \ . \tag{4.23}$$

The path $\{s_i\}$ is given in terms of the Monte Carlo integration variables $\{w_i\}$, $i=1,\ldots,n-1, n+1,\ldots,N-1$ by

$$s_i = \frac{(n-i)s_{i-1} + s_n}{n - i - 1} + (\frac{2\pi\hbar^2\beta}{mN} \frac{n-i}{n-i+1})^{1/2} z(w_i) \tag{4.24a}$$

for $i=1,\ldots,n-1$, and

$$s_i = \frac{(N-i)s_{i-1} + s_0}{N - i - 1} + (\frac{2\pi\hbar^2\beta}{mN} \frac{N-i}{N-i+1})^{1/2} z(w_i) \tag{4.24b}$$

for i=n+1,...,N-1; s_0 and s_n are specified values chosen so that the second partial derivitive with respect s is calculated by finite differences, i.e.

$$\frac{\partial^2}{\partial s_0 \partial s_n} f(s_0,s_n) = \frac{1}{4\varepsilon^2}[f(\varepsilon,\varepsilon) - f(-\varepsilon,\varepsilon) - f(\varepsilon,-\varepsilon) + f(-\varepsilon,-\varepsilon)] \ . \tag{4.25}$$

where each of the four terms are calculated using the same set of random numbers $\{w_i\}$. Thus, if M is the total number of Monte Carlo walks, and the value of $C_f(\tau_n)$ generated by a single walk is denoted as $C_f(\tau_n)_m$, then the Monte Carlo estimate $<C_f(\tau_n)>$ is given by

$$<C_f(\tau_n)> = \frac{1}{m} \sum_{m=1}^{M} C_f(\tau_n)_m \ , \tag{4.26}$$

and the Monte Carlo estimate of the error $\delta C_f(\tau_n)$ is given by

$$\delta C_f(\tau_n) = \frac{\{ \frac{1}{M} \sum_{m=1}^{M} [C_f(\tau_n)_m - <C_f(\tau_n)>]^2 \}^{1/2}}{M^{1/2}} \ . \tag{4.27}$$

Note that the numerator of this expression becomes constant for large M, so the error decreases as $M^{1/2}$ for large M, a well known property of Monte Carlo integration.

b. The Cartesian Reaction Hamiltonian and Influence Functional

We now introduce a "cartesian reaction path Hamiltonian," that is closely related to a model Hamiltonian that has recently been developed and applied to hydrogen atom transfer reactions[43]. It permits an efficient evaluation of the Feynman influence functional. The form of the Hamiltonian is

$$H = T(p_s,\{P_k\}) + V(s,\{Q_k\}) = \frac{p_s^2}{2m} + \sum_k \frac{P_k^2}{2m} + V(s,\{Q_k\}) \ , \tag{4.28}$$

where the potential energy function is

$$V(s,\{Q_k\}) = V_0(s)+\sum_k \frac{1}{2} V_2^k(s)[Q_k - Q_k^0(s)]^2 . \tag{4.29}$$

This model for the potential energy function is that of a harmonic valley (in F−1 dimensions) about a curved reaction path in the F dimensional space, much in the spirit of the reaction path Hamiltonian. The principle difference with the latter is that here the coupling between the reaction coordinate s and the "bath" modes $\{Q_k\}$ is via cross terms in the potential energy in eqn (4.29), rather than in the kinetic energy as for the reaction path Hamiltonian.

In order that this model of the potential energy be able to represent the dynamics of a gas phase bimolecular reaction certain constraints must be imposed on the functions. These constraints are that $V_0(s)$ and $V_2^k(s)$ must become constant asymptotically, and $Q_k^0(s)$ must attain constant slope. Thus in the reactant/product regions of the potential surface there is no coupling between the internal degrees of freedom, and the translational degree of freedom. To illustrate this point more clearly, consider the potential for one orthogonal degree of freedom for large s, which can be represented as

$$\begin{aligned} V(s,Q) &= \frac{1}{2} V_2(Q - \alpha\, s)^2 \\ &= \frac{1}{2} V_2(Q^2 - 2\alpha s Q + \alpha^2 s^2) , \end{aligned} \tag{4.30}$$

where α is the asymptotic slope of $Q^0(s)$. This quadratic form in s and Q can be diagonalized to yield two eigenvalues and eigenvectors. There will be one eigenvalue of frequency zero pointing along the valley of V(s,Q), i.e. with a slope of α, and another eigenvalue with $V_2^{eff} = V_2(1+\alpha^2)$ which is the frequency of the internal mode at the reactant/product geometry. When there is more than one

orthogonal degree of freedom the diagonalization will lead to a more complex set of eigenvalues and eigenvectors, but there will always be one eigenvalue of zero frequency pointing along the reaction path valley. Thus constant asymptotic slope of Q_k^0 guarantees a translational degree of freedom for separation of reacting fragments.

This Hamiltonian does not incorporate the Coriolis-like coupling between the orthogonal modes and the reaction coordinate that would be present if the frequency matrix $V_2^k(s)$ were not constrained to be diagonal. However, the influence functional calculation would be more complicated if this constraint was not imposed.

Next, we will show how the influence functional can be obtained in an efficient procedure. The notation in the next section will be more complicated than previously, since the coordinates Q are labelled by both path step (i) and degree of freedom (k). To keep these labels separate, we denote k as a superscript and i as a subscript.

We now substitute the potential defined in eqn (4.29) into the expression for the influence functional given by eqn (4.20), yielding

$$Z_Q[s(\tau)] = \exp[-\beta/N\sum_{i=1}^{N} V_0(s_i)] \prod_{k=1}^{F-1} \int dQ_0^k \cdots \int dQ_{N-1}^k$$

$$\exp[-\frac{mN}{2\pi\hbar^2\beta}\sum_{i=1}^{N} |Q_i^k - Q_{i-1}^k|^2 - \beta/N\sum_{i=1}^{N} (1/2)V_2(s_i)[Q_i^k - Q_k^0(s_i)]^2 , \qquad (4.31)$$

where we have changed from the rectangular rule to the trapezoid rule in the integration of the potential term.

Note that when F=1 (i.e. when there is only one degree of freedom, that being the reaction coordinate) the one dimensional expression is recovered. Now we need to perform the integrals over the Q_i^k variables. Since the path s_i is given, this is a

gaussian integral, i.e. the exponential factor is of degree two or less in Q_i^k. In general any multidimensional gaussian integral can be evaluated using the formula

$$\int \cdots \int dx \, \exp\{-(\mathbf{x}\cdot\mathbf{A}\cdot\mathbf{x} + \mathbf{b}\cdot\mathbf{x})\} = \frac{\pi^{N/2}}{(\det A)^{(1/2)}} \exp[\frac{\mathbf{b}\cdot\mathbf{A}^{-1}\cdot\mathbf{b}}{4}] \, . \tag{4.32}$$

Straight forward application of the integral formula will not yield an efficient computational scheme. To see this, consider the quantitues that must be computed, and the schemes available for their computation. The matrix A is of rank M where $M = (F-1)\cdot(N-1)$. The most efficient way to obtain the determinent of a general large matrix is to diagonalize it to obtain its eigenvalues, and then to take their product. The computational time taken to diagonalize a matrix scales as M^3. Similiarly, the most efficient way to obtain the term $\mathbf{b}\cdot\mathbf{A}^{-1}\cdot\mathbf{b}$ is to first solve the M dimensional system of linear equations $\mathbf{A}\cdot\mathbf{c} = \mathbf{b}$ for $\mathbf{c}$, which gives $\mathbf{c} = \mathbf{A}^{-1}\cdot\mathbf{b}$. For an arbitrary matrix A, this procedure also scales as M^3. Thus since 30 path steps are typically needed in the path discretization, the calculation cost would scale as $[30(F-1)]^3$. This becomes large rapidly with F and even for F=2 this scheme is impractical.

Progress can be made if we consider the structure of the matrix **A**. The first thing to notice is that it is block diagonal in k. This is a consequence of the constraint that the frequency matrix remain diagonal. This helps since it allows us to treat each degree of freedom independantly. The determinant of a block diagonal matrix is the product of the determinants of each block, and the term $\mathbf{b}\cdot\mathbf{A}^{-1}\cdot\mathbf{b}$ becomes a sum of the contributions from each block independently. Since the $\mathbf{b}\cdot\mathbf{A}^{-1}\cdot\mathbf{b}$ factor occurs inside an exponent, we see that both of these contributions take the form of the product of contributions from each degree of freedom. This is also indicated by the way that eqn (4.31) has been written as a product of factors.

Rewriting eqn (4.31) we have

$$Z_Q[s(\tau)] = \exp[-\beta/N\sum_{i=1}^{N} V_0(s_i)] \prod_{k=1}^{F-1} Y_k[s(\tau)] \ , \tag{4.33}$$

with

$$Y_k[s(\tau)] = \int dQ_0^k \cdots \int dQ_{N-1}^k$$

$$\exp\{ -\frac{mN}{2\pi\hbar^2\beta}\sum_{i=1}^{N} |Q_i^k - Q_{i-1}^k|^2 - \beta/2N\sum_{i=1}^{N} V_2(s_i)[Q_i^k - Q_k^0(s_i)]^2 \} \ . \tag{4.34}$$

Now we consider the evaluation of a single term $Y_k[s(\tau)]$. We can drop the label k for convenience. Recalling that $Q_N = Q_0$, we see that the quadratic form in the exponent of the integral over the variables $Q_0 \rightarrow Q_{N-1}$ is tridiagonal except for the terms in $Q_0 Q_{N-1}$. Since, as will be outlined below, there exist efficient numerical algorithms that scale linearly with size to handle tridiagonal matrices, we want to take advantage or them. The most obvious way to do this is to first perform the integrals over $Q_1 \rightarrow Q_{N-1}$ (but not Q_0), since the quadratic form involving these coordinates is tridiagonal. This leaves an integral over Q_0 which is again gaussian, and so can be done explicitly. Thus we have

$$Y[s(\tau)] = \int dQ_0 \int d\mathbf{q} \exp(-[\mathbf{q}\cdot\mathbf{A}\cdot\mathbf{q} + \mathbf{b}\cdot\mathbf{q} + C + Q_0\mathbf{d}\cdot\mathbf{q} + fQ_0^2 + gQ_0]) \ , \tag{4.35}$$

where $\mathbf{q}=(Q_1 , \ldots , Q_{N-1})$ and all the other new quantities are defined by

$$A_{ij} = [\frac{mN}{\hbar^2\beta} + \frac{\beta}{2N} V_2(s_k)]\delta_{ij} - \frac{mN}{2\hbar^2\beta}(\delta_{i+1,l} + \delta_{i-1,l}) \ , \tag{4.36a}$$

$$b_i = -\frac{\beta}{N} V_2(s_i) Q^0(s_i) \ , \tag{4.36b}$$

$$C = \sum_{i=1}^{N} \frac{\beta}{2N} V_2(s_i) Q^0(s_i)^2 \ , \tag{4.36c}$$

$$d_i = \frac{mN}{\hbar^2\beta}(\delta_{i,1} + \delta_{i,N-1}) \ , \tag{4.36d}$$

$$f = \frac{mN}{\hbar^2\beta} + \frac{\beta}{2N}V_2(s_0) \ , \tag{4.36e}$$

$$g = -\frac{\beta}{N}V_2(s_0)Q^0(s_0) \ . \tag{4.36f}$$

Performing the integral over **q** yields

$$Y = \frac{\pi^{(N-1)/2}}{[\det A]^{1/2}} \int dQ_0 \exp[(\mathbf{b} + Q_0\mathbf{d})\mathbf{A}^{-1}(\mathbf{b} + Q_0\mathbf{d})/4 - c - fq_0^2 - gQ_0] \ . \tag{4.37}$$

This expression is quadratic in Q_0, and can be integrated to yield

$$Y = \frac{\pi^{(N-1)/2}}{[\det A]^{1/2}h^{1/2}} \exp[\ (\mathbf{b}\mathbf{A}^{-1}\mathbf{b} + k^2/h\ )/4 - C\ ] \ , \tag{4.38}$$

where h and k are defined by

$$h = f - \mathbf{d}\mathbf{A}^{-1}\mathbf{d}/4 \ , \tag{4.39a}$$

$$k = g - (\ \mathbf{d}\mathbf{A}^{-1}\mathbf{d} + \mathbf{b}\mathbf{A}^{-1}\mathbf{d}\ )/4 \ . \tag{4.39b}$$

Finally we show how to obtain det **A**, and terms like $\mathbf{A}^{-1}\mathbf{b}$ efficiently, making use of the fact that **A** is a tridiagonal matrix. All of the off-diagonal elements of **A** are identical, and so will be denoted as α. Now denoting as D_i the determinant of the submatrix of rank i, it is easy to see that

$$D_1 = A_{11} \ , \tag{4.40a}$$

$$D_2 = A_{22}D_1 - \alpha^2 \ , \tag{4.40b}$$

and for i>2,

$$D_i = A_{ii}D_{i-1} - \alpha^2 D_{i-2} \,. \tag{4.40c}$$

Thus, in a number of operations linear with N, the determinent is obtained. For large N this step can involve computer overflow errors, but this is easily handled by renormalizing the terms and absorbing the renormalization factor as it logarithm in the exponent.

Finally, as discussed previously, terms such as $\mathbf{A}^{-1}\mathbf{b}$ are obtained by solving the system of linear equations $\mathbf{Ac} = \mathbf{b}$ for $\mathbf{c}$. For a tridiagonal $\mathbf{A}$, this is done easily by gaussian elimination of the off diagonal elements sequentially. First $A_{i+1,i}$ is eliminated using row i from i=1, $\cdots$,N–2, leaving each row with two elements (A_{ii},$A_{i,i+1}$) except for row N-1 which now contains only the diagonal element. Then $A_{i,i+1}$ is eliminated using row i+1 from i=n–2, $\cdots$,1. This procedure is again linear with N.

Thus we can obtain the influence functional for arbitrary dimensionality and number of path discretizations in a numerical procedure that scales linearly with both of these variables.

c. Utility of the Influence Functional

In the previous section an efficient method of obtaining the influence functional within the framework of the cartesian reaction path Hamiltonian has been developed. However, it was noted that a restriction on the form of the potential (neglect of the off diagonal terms in the potential expansion) had to be imposed in order to obtain an efficient calculational method.

There may be situations where this approximation is not justified, which raises the question of whether an influence functional approach is appropriate in such situations, or whether it would be better to evaluate the entire integral by the Monte Carlo procedure. Although this question cannot be answered in general, some of the

considerations involved will be briefly discussed.

Consider a general integral that we wish to evaluate by Monte Carlo, which will be written as

$$\mathbf{I} = \int dx \int dy\ f(\mathbf{x},\mathbf{y}) \ , \tag{4.41}$$

and assume that at some computational cost we can do the integral over **y**, i.e. we can obtain

$$g(\mathbf{x}) = \int dy\ f(\mathbf{x},\mathbf{y}) \ . \tag{4.42}$$

We now have two possible stategies for the Monte Carlo evaluation of **I**: we could evaluate eqn (4.41) directly by sampling in both **x** and **y** space, or we could make us of eqn (4.42), and obtain **I** as

$$\mathbf{I} = \int dx\ g(\mathbf{x}) \tag{4.43}$$

by sampling only in **x** space. Influence functional approaches correspond to making the second choice. It seems clear that if the computational cost of obtaining g(**x**) is not prohibitive, the second approach would be preferred. This is the situation described in the previous section.

Now we consider the case where the evaluation of g(**x**) is computationally expensive. The Monte Carlo error in the evaluation of **I** by the two methods is given by

$$\delta I_f = \frac{<<f^2>>^{1/2}}{N_f^{1/2}} \ ,$$

$$\delta I_g = \frac{<<g^2>>^{1/2}}{N_g^{1/2}} \ , \tag{4.44}$$

where N_f and N_g are the number of Monte Carlo samples, and the intrinsic variance is defined by

$$<<g^2>> = \int dx\ g(x)^2 - |\int dx\ g(x)|^2 , \tag{4.45}$$

and similiarily for $<<f^2>>$, except the integrals range over both x, and y for this case.

Now in general $<<f^2>> \geq <<g^2>>$, so that if g costs the same to evaluate as f, making use of g is preferred. However, if g is expensive to compute this may no longer be true. Thus, depending on the intrinsic variance of f and g and the computational cost of obtaining g, either method may be preferred.

d. Analytic Continuation Methods

To this point in the chapter we have described a procedure that allows us to obtain values of the reactive flux correlation function for purely imaginary times, but of course the rate constant is given as the integral of the correlation function over purely real times from zero to infinity. Thus, some method of analytically continuing from imaginary to real time values of $C_f(t)$ must be developed.

In past work in this group[8,39,40], this was accomplished by using Schlessinger's[44] point method which generates a continued fraction that reproduces all the imaginary time values of the correlation function exactly. Then making the replacement $t = i\tau$ generates the real time values.

This procedure does not correctly account for the finite Monte Carlo error in the values of $C_f(\tau)$. Thus, below we will describe two methods that we have found to be useful analytic continuation procedures. These methods differ from the previous approach in that instead of reproducing the imaginary time Monte Carlo estimates exactly, they are represented to within the accuracy justified by their

statistical uncertainty.

The first method is very much in the spirit of a minimal transition state theory. As we have seen from previous calculations where the dynamics is direct (one dimensional eckart barrier and collinear $H+H_2$ examples), the correlation function decays to zero very quickly, and in times of less than $(\hbar\beta/2)$ where tunneling is important. Thus, a very good estimate of the rate constant could be obtained by considering only the value of $C_f(t)$ at time zero, and its decay width. (This contrasts with classical transition state theory, where the correlation function has no width, so that only the zero time value is required.)

Another consideration that must be included is the known structure of $C_f(t)$ in the complex plane. The continuation function must incorporate the singular behavior at $t = \pm\hbar\beta/2$. The first function we used is

$$C_f(t) = \frac{C\,(\hbar\beta/2)^2}{[\,t^2 + (\hbar\beta/2)^2]^{3/2}}\,\exp(\,-bt^2)\,. \tag{4.46}$$

The parameters C and b are obtained by fitting the analytically continued version of this expression (obtained by the substitution $t = i\tau$) to the values of $C_f(\tau)$ obtained by the Monte Carlo procedure described previously, i.e. we fit to the expression

$$C_f(\tau) = \frac{C\,(\hbar\beta/2)^2}{[\,(\hbar\beta/2)^2 - \tau^2\,]^{3/2}}\,\exp(\,b\tau^2)\,. \tag{4.47}$$

We note that the first factor correctly incorporates the singularities at $\tau = \pm\hbar\beta/2$, while the gaussian is an entire function, and so has no poles anywhere. The advantage of the gaussian is that for positive exponent b (an essential restriction), the real time behavior is guaranteed to decay faster than the free particle result. Thus, we have a functional form characterized by two parameters which yields a valid approximation to the short time behavior of $C_f(t)$. The parameters are

determined by weighted least squares fitting to the Monte Carlo values of $C_f(\tau)$ (with the weights determined by the Monte Carlo error). Finally the rate is determined by numerically integrating the fitting function out to $t = 5\hbar\beta$, where $C_f(t)$ is negligible for the free particle reference.

The second method is quite similiar to the first one, but can be used when the Monte Carlo error is small enough to justify a more precise fit. In this method we assume that $C_f(t)$ can be described by

$$C_f(t) = \frac{kT}{h} \frac{(\hbar\beta/2)^2}{[t^2 + (\hbar\beta/2)^2]^{3/2}} \frac{1}{[\sum_{n=0}^{N} a_n t^{2n}]} . \tag{4.48}$$

The two parameter version of this is similiar to the exponential described above, while additional parameters can lead to a more accurate representation if justified by the Monte Carlo error. In using this method we increase the number of parameters until the average deviation between the fitted expression and calcutated expression is within the Monte Carlo error bars. To be more precise, denoting the Monte Carlo value by $<C_f(\tau_n)>$, and the fitted value by $C_f(\tau_n)$, the average deviation is defined by

$$d = \frac{1}{N} \sum_{n=1}^{N} \frac{[<C_f(\tau_n)> - C_f(\tau n)]^2}{[\delta C_f(\tau_n)]^2} . \tag{4.49}$$

The number of fitting parameters is increased until $d < 1$. This second method is similiar to Schlessinger's point method except that the number of parameters is determined by the precision of the Monte Carlo estimates, instead of the number of τ values for which $C_f(\tau)$ was obtained.

3. *APPLICATION TO THE COLINEAR* $H+H_2$ *SYSTEM*

In this section the methods developed in the last section will be applied to the collinear $H + H_2$ reaction to test the various approximations. There are three new methods described is the previous section. In what follows we will demonstrate the validity of the cartesian reacton path Hamiltonian approximation, the accuracy or the influence functional calculation, and the analytic continuation method.

Consider now the cartesian reaction path approximation to the potential for collinear $H + H_2$. For this reaction, two symmetrically identical $H + H_2$ channels move away from the transition state at an angle of 60° to each other (recall eqn (3.4): $\theta_m = \tan^{-1}[3^{1/2}] = 60°$). The cartesian reaction coordinates are defined by the transition state geometry, i.e. the coordinate s is the reaction coordinate and corresponds to the asymmetric stretch, while Q is the orthogonal coordinate and corresponds to the symmetric stretch. The situation is depicted in figure 15, where the $H + H_2$ surface is shown in relation to the coordinate system (s,Q). Using figure 15 we can also see how the cartesian reaction potential functions $V_0(s)$, $V_2(s)$, and $Q_0(s)$ are obtained. At any given $s = s_0$, $V(s_0,Q)$ is minimized with respect to Q, to obtain $Q_0(s_0)$. Doing this for all s_0 yields the function $Q_0(s)$. Then $V_0(s)$ and $V_2(s)$ are given by:

$$V_0(s) = V(s,Q_0(s)) \ ,$$

$$V_2(s) = \frac{\partial^2}{\partial Q^2} V(s,Q)\,|_{Q = Q_0(s)} \ . \tag{4.50}$$

The cartesian reaction path potential functions are shown in figure 16.

Note that although the frequency at the transition state is much lower than the asymptotic frequency (2813 cm^{-1} vs 4395 cm^{-1}), the function $V_2(s)$ does not vary

by nearly as much. This is because the asymptotic frequency is given by $V_2(1 + \alpha^2)$ where α is the slope of $Q_0(s)$. (In this case $\alpha = 3^{1/2}$.) The function $Q_0(s)$ shows the reaction path curvature through the interaction region.

At this point it is useful to mention the role of anharmonicities in the potential. Our model assumes that the potential can be expanded as a harmonic valley about the reaction path. This is of course an approxination. For example for $H + H_2$ at 200 K, the transition state theory rate constant obtained using the Porter-Karplus surface with Morse oscillator partition functions for the activated complex and reactant oscillator is $2.03 \cdot 10^{-2}$ cm/sec, while the transition state theory rate obtained using harmonic oscillator partition functions is $2.42 \cdot 10^{-2}$ cm/sec, i.e. the harmonic approximation overestimates the rate by 20%. The origin of this error is simple to understand. At low temperature an oscillator partition function is given by $\exp(-\beta\varepsilon_0)$ where ε_0 is the zero point motion energy. Both reactant and activated complex zero point motion energies are too high in the harmonic approxination, since anharmonicity lowers zero point energy. However, since the reactant frequency is higher than the transition state frequency, the error is higher there. Thus, the effective barrier to reaction ({bare barrier} + {transitiuon state zero point motion} - {reactant zero point motion}) is too low in the harmonic approximation, so the rate constant is overestimated. This problem can be avoided if the transition state expression is calculated using accurate partition functions that use the correct zero point motion motion, and only the correction to transition state theory "κ" is calculated in the harmonic approximation.

In Chapter 3, the basis set method for collinear reactions was described. We used this method to calculate κ for both the Porter-Karplus surface, and the cartesian reaction path approximation to it at several temperatures. Using the cartesian reaction path potential, the values of κ obtained for the temperatures 200 K, 300 K,

600 K, and 1000 K were respectively 48, 9.0, 2.5, and 1.6. This compares with the values obtained in Chapter 3 which were 46, 8.7, 2.5, and 1.5. Thus, in this case the harmonic approximation to the potential is very accurate for the purpose of calculating the correction to transition state theory. It is worth noting that the differences between the correct quantum correction factors and the ones obtained using the harmonic approximation to the potential are less than the differences in the transition state theory rates between the two potentials.

Next the accuracy of the path integral calculation in the calculation of imaginary time values of the reactive flux correlation function is demonstrated. Again we can compare the path integral method with the basis set method by using the latter method to calculate correct valus of $C_f(\tau)$. The basis set expression is

$$C_f(\tau) = \sum_{nn'} \exp[(-\beta/2 + \tau/\hbar)\, E_n\,] \exp[(-\beta/2 - \tau/\hbar)\, E_{n'}]\, |\langle n|F|n'\rangle|^2 \,. \qquad (4.51)$$

For $-\hbar\beta/2 < \tau < \hbar\beta/2$ this expression converges for finite basis sets. Outside of this range the expression is not well behaved (since one of the exponential terms diverges). This corresponds to the real behavior of $C_f(\tau)$.

In the discussion of the basis set method for real time calculations (Chapter 2 section 3) we pointed out the fact that this method could never be accurate out to infinite time. However, by using a particle in a box basis set, accurate results could be obtained for progressively longer times by increasing the box size. Similiarly, the accuracy of the imaginary time values is related to the length of real time over which the correlation function behaves correctly, i.e. the best values of $C_f(\tau)$ are obtained from a basis set calculation where $C_f(\tau)$ goes to zero and stays there for a long time before the wall recrossing occurs. This makes sense, and can be shown to be true for the one-dimensional free particle correlation function where the (analytic) basis set expression for $C_f(\tau)$ can be compared to the analytic functional form.

We have thus calculated the imaginary time values of the reactive flux correlation function for the range of temperatures used above, and compared them with the basis set results. At high temperatures (T=600 K,1000 K), where the quantum correction is close to 1, we can obtain accurate results with 30 path discretization steps, and 1000 Monte Carlo integration points. In fact for these cases it is easier to obtain the imaginary time correlation function with the path integral method than the basis set method because of reflection of flux off the walls in the basis set method. This flux reflection occurs earlier at higher temperatures because the average kinetic energy is higher. To obtain accurate results at T=300 K, 60 path steps, and 10,000 Monte Carlo walks were used, while at T=200 K these numbers were 90, and 30,000 respectively. In Table 3 we present results of the path integral influence functional calculations of $C_f(\tau)$ for the lowest temperature used above (T=200 K) for various values of τ. Also listed in Table 3 are the Monte Carlo error estimates, and the values of $C_f(\tau)$ obtained using the basis set method. The Monte Carlo estimates agree with the basis set results within the error bars (i.e. 68% of the Monte Carlo results should be within one error bar of the basis set results), but also systematically slightly overestimate the basis set results. This effect increases with τ, and so may also be an artifact of flux recrossing in the basis set calculation.

The increased variance at low temperatures can be understood in terms of the random walk algorithm described in section 2 (eqn (4.24)). The average size of step taken increases as temperature decreases. Since all walks begin and end on the dividing surface which was chosen to be at the maximum of $V_0(s)$, small excursions sample a region that is roughly constant. As temperature decreases the walks probe a larger region of the potential, and so the sampled region is much less constant, requiring more Monte Carlo points to obtain the same error. The reason for the increase in the number of path discretization steps is similiar. By increasing the number of points, the step size decreases, so that the trapezoid rule integration of the

potential term becomes more accurate.

Finally, for the calculations discussed above, the results of the analytic continuation procedure are shown in Table 4. The two methods described in section 2.c are used. While the simple gaussian method works for high temperatures where the fit results in $b \approx 0$ (since the correlation function shape is well approximated by the free particle reference), it overestimates the rate for low temperatures. Even in these cases it may be useful since the lack of flexibility also gives increased stability, so that while the rate may not be precisely correct, it is also bounded in its deviation from the correct value. The inverse polynomial method generates more accurate results for the low temperature cases and gives the quantum correction to within 10% of the basis set value. Thus, when the accuracy of the Monte estimates justify more than two parameters this method should be used.

4. DISCUSSION

We have developed a path integral influence functional method for calculating imaginary time values of the flux correlation function, and a consistent method of analytically continuing the correlation function to real times to obtain the correction to transition state theory. Application of this method to the colinear $H + H_2$ reaction gave good results. The utility of the method lies in the fact that the cost of calculations for multidimensional systems scales linearly with the number of dimensions, so that these calculation are feasible.

However, the method has some obvious limitations. In Chapter 3 we performed basis set calculations on three different collinear reactions. Of these three only the $H + H_2$ reaction could be treated by the method of this chapter. This is because the correction to transition state theory for this reaction is entirely due to tunneling. Direct tunneling through a barrier happens in a short time, and thus is

incorporated in the initial, lobe of $C_f(t)$, which the present method estimates.

For the Cl + HCl reaction, the major correction to transition state theory is due to classical recrossing, a long time phenomenon not treated correctly by the present procedure. Note however, that since this recrossing is a classical effect it can be treated in a classical trajectory calculation as in Chapter 3.

For the $F + F_2$ reaction the limitations of the present approach are more severe, and are due to the fact that the potential surface is not symmetric. First of all, the nonsymmetric version of the coordinate representation of the flux correlation function must be used, a minor change. The second point is concerned with the fact that to obtain the results in Chapter 3 it was necessary to project out eigenstates that could not exist asymptotically as reactant states from the correlation function expression. This projection is natural in a basis set calculation, but cannot be done in a path integral calculation. Since this projection may be necessary for any non symmetric reaction, this severely limits the utility of path integral approachs to these problems.

Another problem with treating the $F + H_2$ reaction using the cartesian reaction path Hamiltonian is the geometry of the potential surface. The transition state occurs early in the entrance channel, and a cartesian coordinate system based on the transition state cannot follow the reaction path without the function $Q_0(s)$ attaining infinite slope and turning back upon itself.

Before making too much of these problems we must recall the purpose of developing the method. We were interested in developing a method to calculate tunneling corrections to transition state theory. This presupposes that the quantum version of the transition state theory assumption be valid, i.e. that the dynamics be direct. For the reaction where the assumption held we were able to obtain accurate results. The discussion of the other two reactions then shows the limitations of

applicability of the transition state theory idea.

In conclusion we can state that this is probably as close to a practical version of transition state theory that one is likely to achieve in quantum mechanics. In classical mechanics transition state theory is a zero time (i.e. no dynamics) theory. The best we can do in quantum mechanics is to obtain a purely imaginary time theory, which can give accurate values of the correlation function for times that correspond to the quantum spreading of the classical delta function.

REFERENCES

[1] See for example: (a) S. Glasstone, K.J. Laidler, H. Eyring, *The Theory of Rate Processes*, McGraw-Hill, New York, 1941; (b) P. Pechukas in *Dynamics of Molecular Collisions*, edited by W.H. Miller, Plenum, New York, 1976, p. 269; (c) D.G. Truhlar, W.L. Hase, J.T. Hynes, J. Chem. Phys. **87**, 2264 (1983).

[2] (a) J.C. Keck, J. Chem. Phys. 32, 1035 (1960); (b) J.C. Keck, Adv. Chem. Phys. **13**, 85 (1967).

[3] D.G. Truhlar and B.C. Garrett, Acc. Chem. Res. **13**, 440 (1980).

[4] E. Wigner, Trans. Faraday Soc **34**, 29 (1938).

[5] B.C. Eu and J. Ross, J. Chem. Phys. **44**, 2467 (1966).

[6] (a) P. Pechukas and F.J. McLafferty, J. Chem. Phys. **58**, 1622 (1973); (b) P. Pechukas and F.J. McLafferty, Chem. Phys. Lett. **27**, 511 (1974).

[7] W.H. Miller, J. Chem. Phys. **61**, 1823 (1974).

[8] W.H. Miller, S.D. Schwartz and J.W. Tromp, J. Chem. Phys. **79**, 4889 (1983).

[9] R.P. Feynman and A.R. Hibbs, *Quantum Mechanics and Path Integrals*, McGraw-Hill, New York, 1965.

[10] I.M.W Smith, *Kinetics and dynamics of elementary gas reactions*, Butterworths, Boston, 1980, pg. 113.

[11] T. Yamamoto, J. Chem. Phys. **33**, 281 (1960).

[12] P.G. Wolynes, Phys. Rev. Lett. **47**, 968 (1981).

[13] R.K. Boyd, Chem. Rev. **77**, 93 (1977).

[14] D. Chandler, J. Chem. Phys. **68**, 2959 (1978).

[15] (a) S.H. Northrup and J.T. Hynes, J. Chem. Phys. **73**, 2700 (1980); (b) R.F. Grote and J.T. Hynes, J. Chem. Phys. **73**, 2715 (1980).

[16] H.S. Johnston, *Gas Phase Reaction Theory*, Ronald, New York 1966, pp 40-42.

[17] J. Costley and P. Pechukas, Chem. Phys. Lett. **83**, 139 (1981).

[18] *CRC Handbook of Chemistry and Physics, 61st edition*, CRC Press, Boca Raton, Florida 1980-81, pp A-60, integral 239.

[19] W.H. Miller, Accts. Chem. Res. **9**, 306 (1976).

[20] W.H. Miller, N.C. Handy and J.E. Adams, J. Chem. Phys. **72**, 99 (1980).

[21] R.N. Porter and M. Karplus, J. Chem. Phys. **40**, 1105 (1964).

[22] G.C. Schatz, J.M. Bowman, J. Dwyer and A. Kuppermann, unpublished, cited in D.G. Truhlar, A. Kuppermann and J. Dwyer, Mol. Phys. **33**, 683 (1973).

[23] D.K. Bondi, D.C. Clary, J.N.L. Connor, B.C. Garrett and D.G. Truhlar, J. Chem. Phys. **76**, 4986 (1982).

[24] D.K. Bondi, J.N.L. Connor, B.C. Garrett and D.G. Truhlar, J. Chem. Phys. **78**, 5981 (1983).

[25] P.A. Whitlock and J.T. Muckerman, J. Chem. Phys. **61**, 4618 (1975).

[26] G.C. Schatz, J.M. Bowman and A.Kuppermann, J. Chem. Phys. **63**, 674 (1975).

[27] B.C. Garrett, D.G. Truhlar, R.S. Grev, A.W. Magnusson and J.N.L. Connor, J. Chem. Phys. **73**, 1721 (1980).

[28] See for example reference 10, pg. 93.

[29] A. Kuppermann, J.A. Kaye and J.P. Dwyer, Chem. Phys. Lett. **74**, 257 (1980).

[30] J. Romelt, Chem. Phys Lett. **74**, 263 (1980).

[31] (a) J.W. Cooley, Math. Computations **15**, 363 (1961); (b) J.K. Cashion, J. Chem. Phys. **39**, 1872 (1963); (c) R.N. Zare, University of California Radiation Laboratory Report UCRL-10925 (1963).

[32] C.C. Rankin and W.H. Miller, J. Chem. Phys. **55**, 3150 (1971).

[33] (a) I.M.W. Smith, J. Chem. Soc. Faraday II **77**, 747 (1981); (b) R.J. Frost and I.W.M. Smith, Chem. Phys. **111**, 389 (1987).

[34] S. Chapman, S.M. Hornstein and W.H. Miller, J. Am. Chem. Soc. **97**, 892 (1975).

[35] E. Pollak and P. Pechukas, J. Chem. Phys. **69**, 1218 (1978).

[36] E. Pollak, M.S. Child and P. Pechukas, J. Chem. Phys. **72**, 1669 (1980).

[37] See for example: J. Romelt and E. Pollak in *Resonances in Electron-Molecule Scattering, van der Waals Complexes and Reactive Chemical Dynamics*, edited by D.G. Truhlar, Amer. Chem. Soc., Washington, D.C., 1984; ACS Symp. Ser. No. 263, pg. 353.

[38] B.A. Waite and W.H. Miller, J. Chem. Phys. **76**, 2412 (1982).

[39] R. Jaquet and W.H. Miller, J. Phys. Chem. **89**, 2139 (1985).

[40] K. Yamashita and W.H. Miller, J. Chem. Phys. **82**, 5475 (1985).

[41] Reference 9, pg. 43.

[42] M. Abramowitz and I.A. Stegun, *Handbook of Mathematical Functions*, U.S. Government Printing Office, Washington, D.C., 1964, pg. 933.

[43] B.A. Ruf and W.H. Miller, J. Chem. Soc. Faraday Trans. **2**, 84 (1988).

[44] L. Schlessinger, Phys. Rev. **167**, 1411 (1968).

TABLE 1

A comparison of the width of one dimensional Eckart barrier correlation functions at different temperatures.

$\hbar\beta/2$	$t_{1/2}$	$t_{1/2}/(\hbar\beta/2)$
1	.75	.75
3	1.41	.47
5	1.53	.30
10	3.7	.37
20	9.8	.49
50	32	.64
100	67	.67
200	144	.72
400	290	.73
800	600	.75

TABLE 2

Comparison of the initial decay of the different collinear reaction quantum correlation functions.

T	$t_{1/2}$	$\hbar\beta/2$	$t_{1/2}/(\hbar\beta/2)$	$\kappa = k^{QM}/k^{TST}$
(a) $H + H_2 \rightarrow H_2 + H$				
200	410	790	.52	46.
300	345	526	.66	8.7
600	210	263	.80	2.5
1000	125	158	.79	1.5
(b) $Cl + HCl \rightarrow ClH + Cl$				
200	630	790	.80	5.3
300	420	526	.80	2.0
600	210	263	.80	.62
1000	120	158	.76	.33
(c) $F + H_2 \rightarrow FH + H$				
200	590	790	.75	.81
300	390	526	.74	.57
600	220	263	.84	.43
1000	160	158	1.01	.40

TABLE 3

Comparison of the Monte Carlo (MC) path integral influence functional calculations of the imaginary time flux correlation function for the collinear $H + H_2$ reaction with Basis Set (BS) calculations at 200 K ($\hbar\beta/2=789.4$). The displayed results were obtained using 90 path discretization steps and 30,000 Monte Carlo random walks.

τ_n	$\langle C_f^{MC}(\tau_n)\rangle$	$\delta C_f^{MC}(\tau_n)$	$C_f^{BS}(\tau_n)$
52.6	.1123	$.23\times10^{-2}$	.1115
157.9	.1227	$.25\times10^{-2}$	.1222
263.1	.1481	$.29\times10^{-2}$	.1472
368.4	.1978	$.41\times10^{-2}$	.1961
473.7	.3010	$.63\times10^{-2}$	.2942
578.9	.5434	$.12\times10^{-1}$	.5253
684.2	1.429	$.32\times10^{-1}$	1.404

TABLE 4

The values of the quantum correction " κ " for the collinear $H + H_2$ reaction obtained by the analytic continuation methods. The methods compared are the inverse polynomial (IP) method and the gaussian (G) method. Also shown are the correct values for this potential surface obtained by the basis set (BS) method.

T	IP	G	BS
200	53.	56.	48.
300	9.0	10.4	9.0
600	2.4	2.6	2.5
1000	1.7	1.6	1.6

FIGURE CAPTIONS

1. A typical one dimensional potential curve (the symmetrical Eckart barrier), with reactants to the left and products to the right. Two different choices of transition state theory dividing surface, $s=0$ (solid vertical line) and $s=s_0$ (dotted vertical line) are shown.

2. The reactive flux correlation function for the one dimensional Eckart barrier with $\alpha=12$. The values of u are indicated on the figure.

3. The time dependent quantum correction $\Gamma(t)$ defined by eqn (2.39b) for the three correlation functions of figure 2. The quantum correction Γ is given by the long time limit of $\Gamma(t)$.

4. The classical (CL) and quantum mechanical (QM) flux correlation functions are shown for the potential of figure 1 for the case that the dividing surface is chosen at the top of the barrier ($s_0=0$) or displaced from it ($s_0\neq0$). The shaded regions in the classical (CL) case indicate delta functions at $t=0$.

5. Same as figure 1, except for an unsymmetrical Eckart potential.

6. (a) and (b) show the quantum flux correlation functions for the potential of figure 5 for the case that $s_0=0$ and $s_0\neq0$, respectively, where the flux operator F is the normal one, eqn (2.20). (c) shows the flux correlation function for the potential of figure 5 for the modified flux operator F_r of eqn (2.44), for the case $s_0 = 0$.

7. A comparison of alternate versions of the reactive flux correlation function for the symmetrical Eckart barrier with $u=8$, $\alpha=12$. (a) The Miller, Schwartz and Tromp correlation function $C_f(t)$ defined by eqn (2.46a). (b) The unsymmetric Boltzmann operator correlation function $C_f^{\lambda}(t)$ defiined by eqn (2.46b). (c) The

Yamamoto correlation function $C_f^K(t)$ defined by eqn (2.46c).

8. The time dependent effective quantum correction factor $\Gamma(t)$ corresponding to each of the correlation functions displayed in figure 7.

9. The quantum mechanical reactive flux correlation function for the $H + H_2 \rightarrow H_2 + H$ reaction, at the indicated temperatures. The displayed correlation functions are all normalized to unity at t=0; i.e., the quantities shown are actually $C_f(t)/C_f(0)$. Note that 1000 atomic units of time ~ 24 femtoseconds.

10. The classical correlation functions for $H + H_2$; see also notes for figure 9.

11. The quantum mechanical correlation functions for the $Cl + HCl \rightarrow ClH + Cl$ reaction; see also notes for figure 9.

12. The classical correlation functions for Cl + HCl; see also notes for figure 9.

13. The quantum mechanical correlation functions for the $F + H_2 \rightarrow FH + H$ reaction; see also notes for figure 9.

14. The classical correlation functions for $F + H_2$; see also notes for figure 9.

15. The cartesian reaction coordinates (s,Q) in relation to equipotential contours of the collinear $H + H_2$ potential surface.

16. The cartesian reaction Hamiltonian functions $V_0(s)$, $V_2(s)$, and $Q_0(s)$ for the Porter-Karplus $H + H_2$ potential.

FIGURE 1

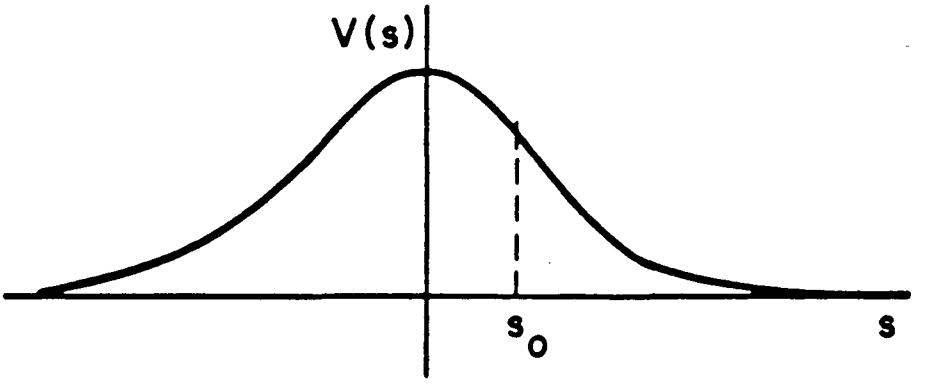

FIGURE 2

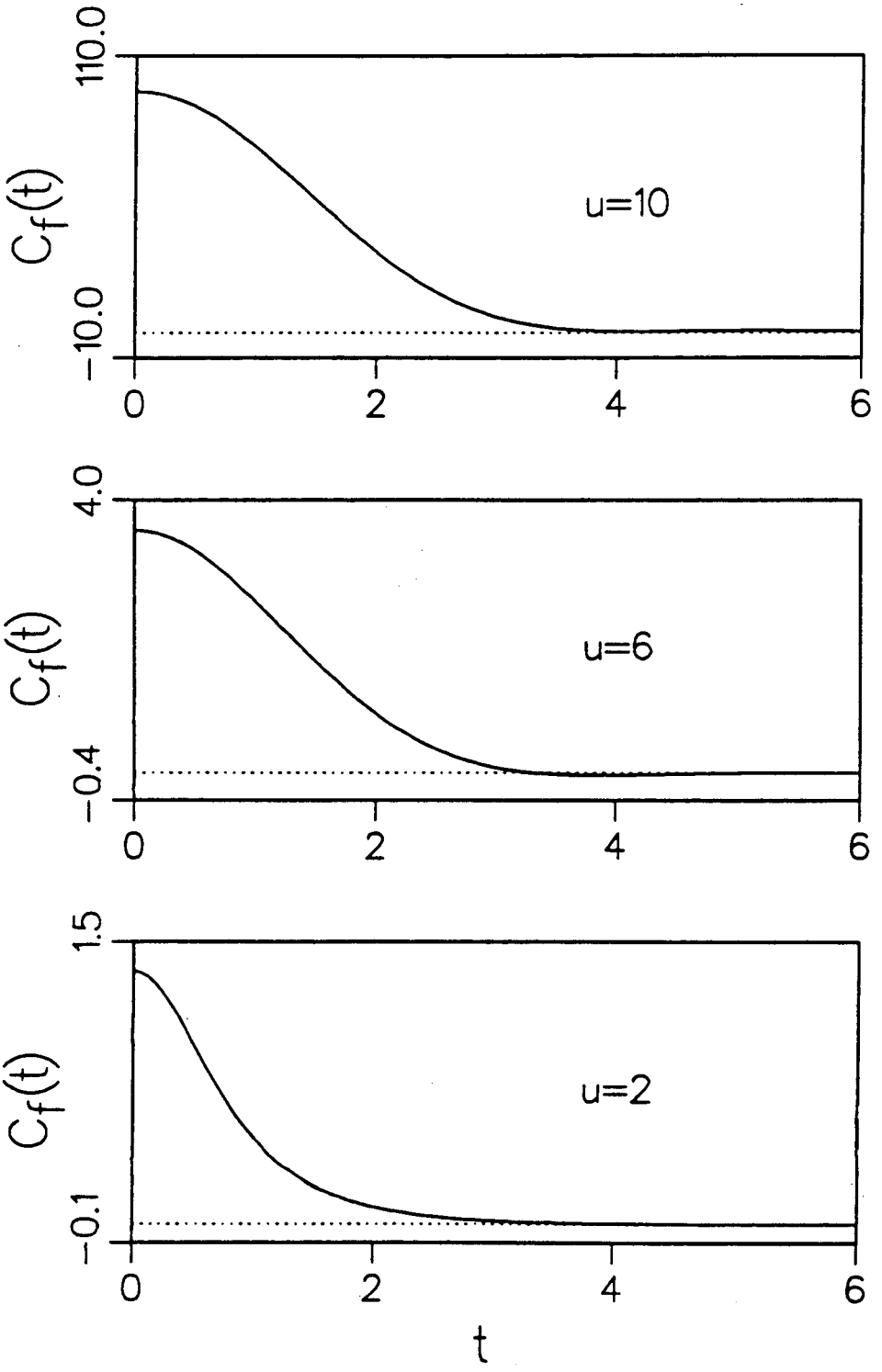

FIGURE 3

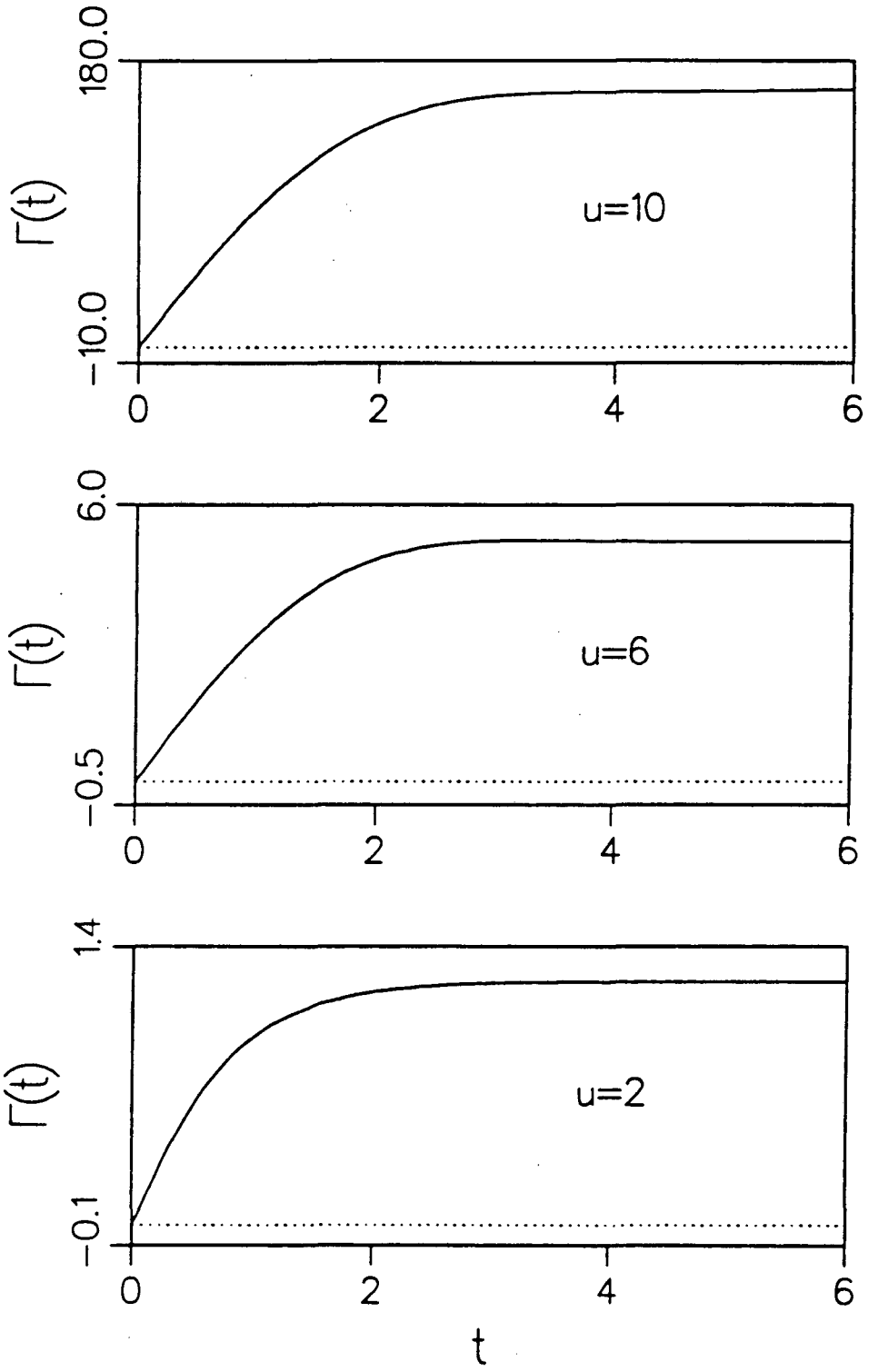

FIGURE 4

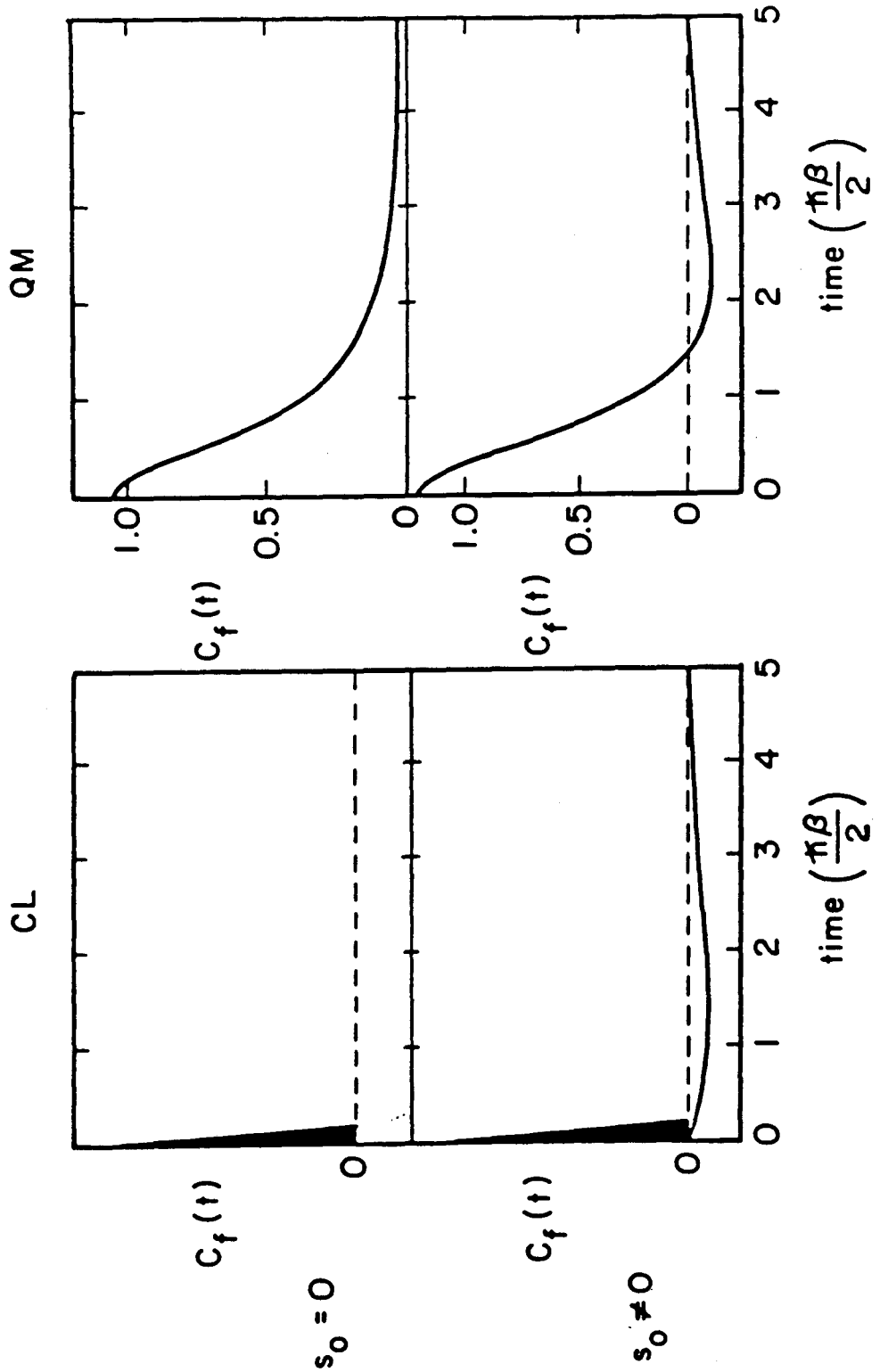
CL
QM
$C_f(t)$
$s_0 = 0$
$s_0 \neq 0$
1.0
0.5
0
0
1
2
3
4
5
time $\left(\frac{\hbar\beta}{2}\right)$

FIGURE 5

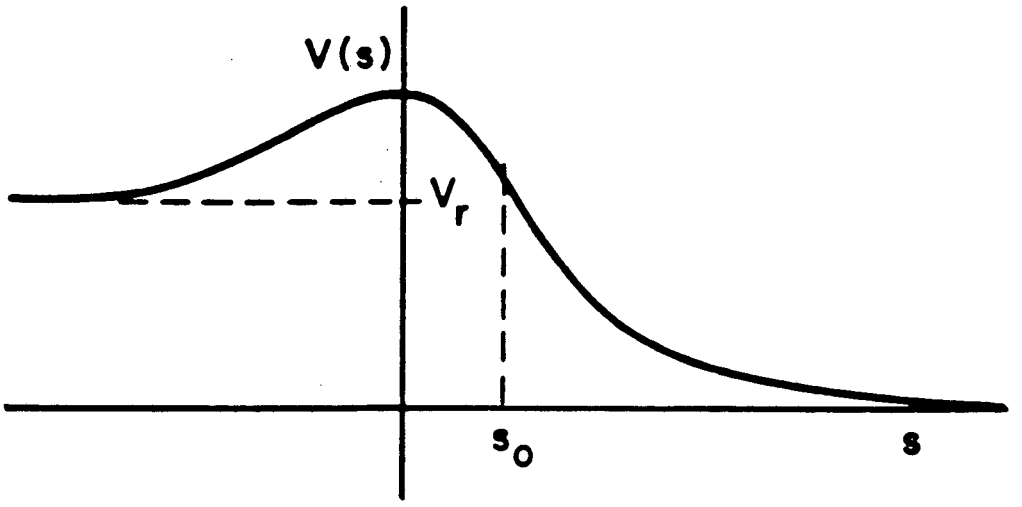

FIGURE 6

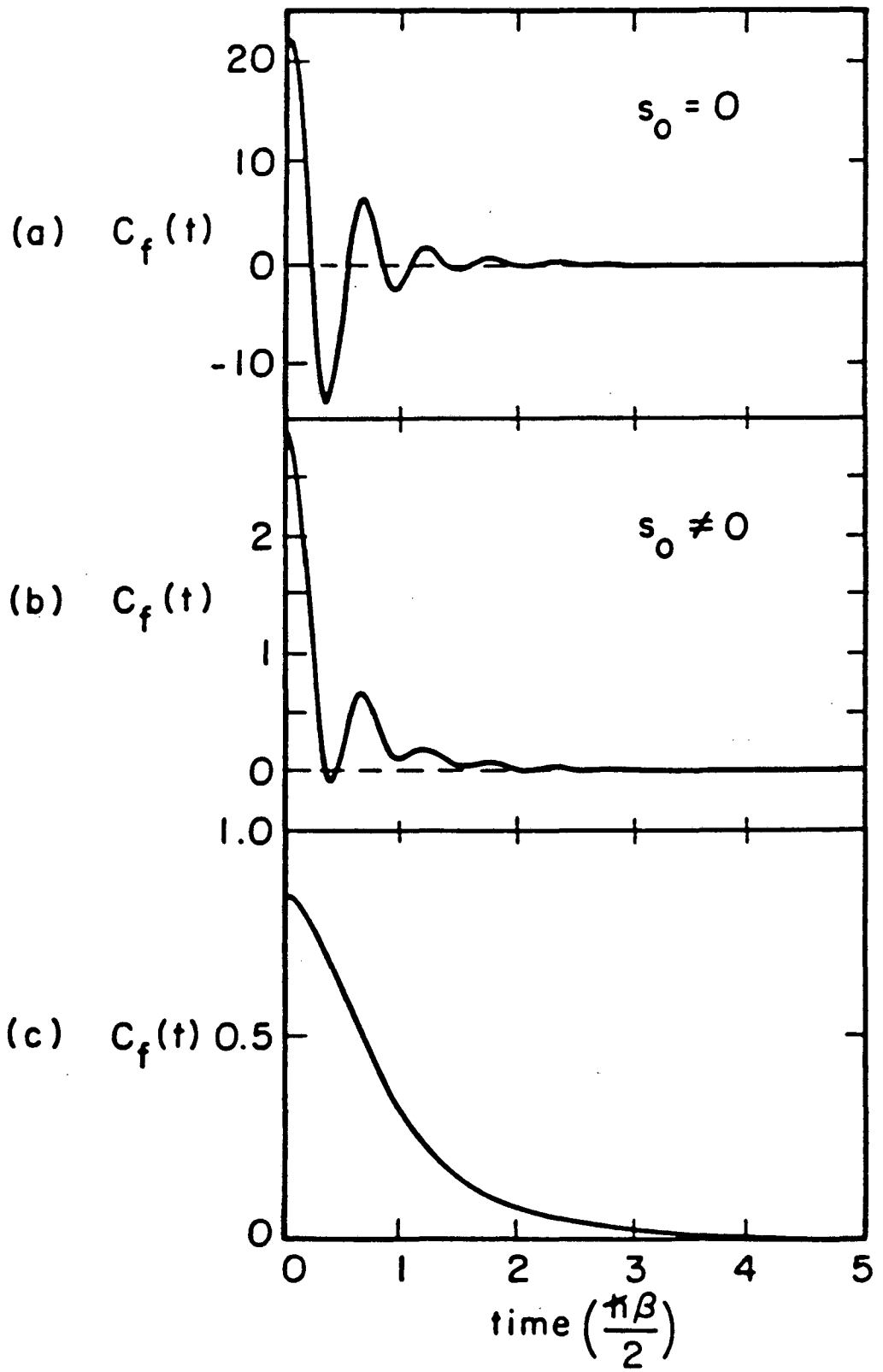
20
10
0
-10
(a) $C_f(t)$
$s_0 = 0$
2
1
0
(b) $C_f(t)$
$s_0 \neq 0$
1.0
0.5
0
(c) $C_f(t)$
0
1
2
3
4
5
time $\left(\frac{\hbar\beta}{2}\right)$

FIGURE 7

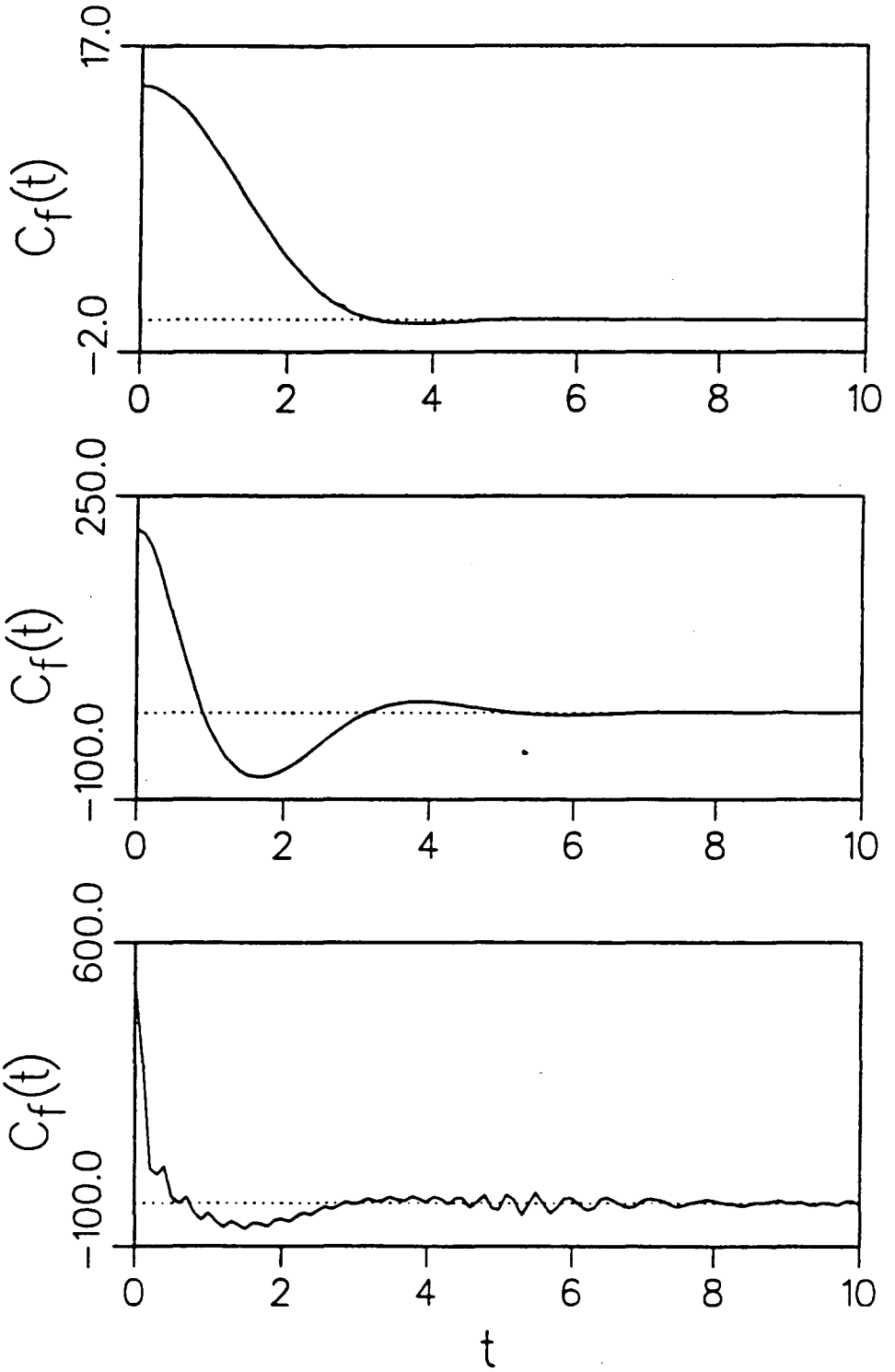
17.0
-2.0
$C_f(t)$
0
2
4
6
8
10
250.0
-100.0
$C_f(t)$
0
2
4
6
8
10
600.0
-100.0
$C_f(t)$
0
2
4
6
8
10
t

FIGURE 8

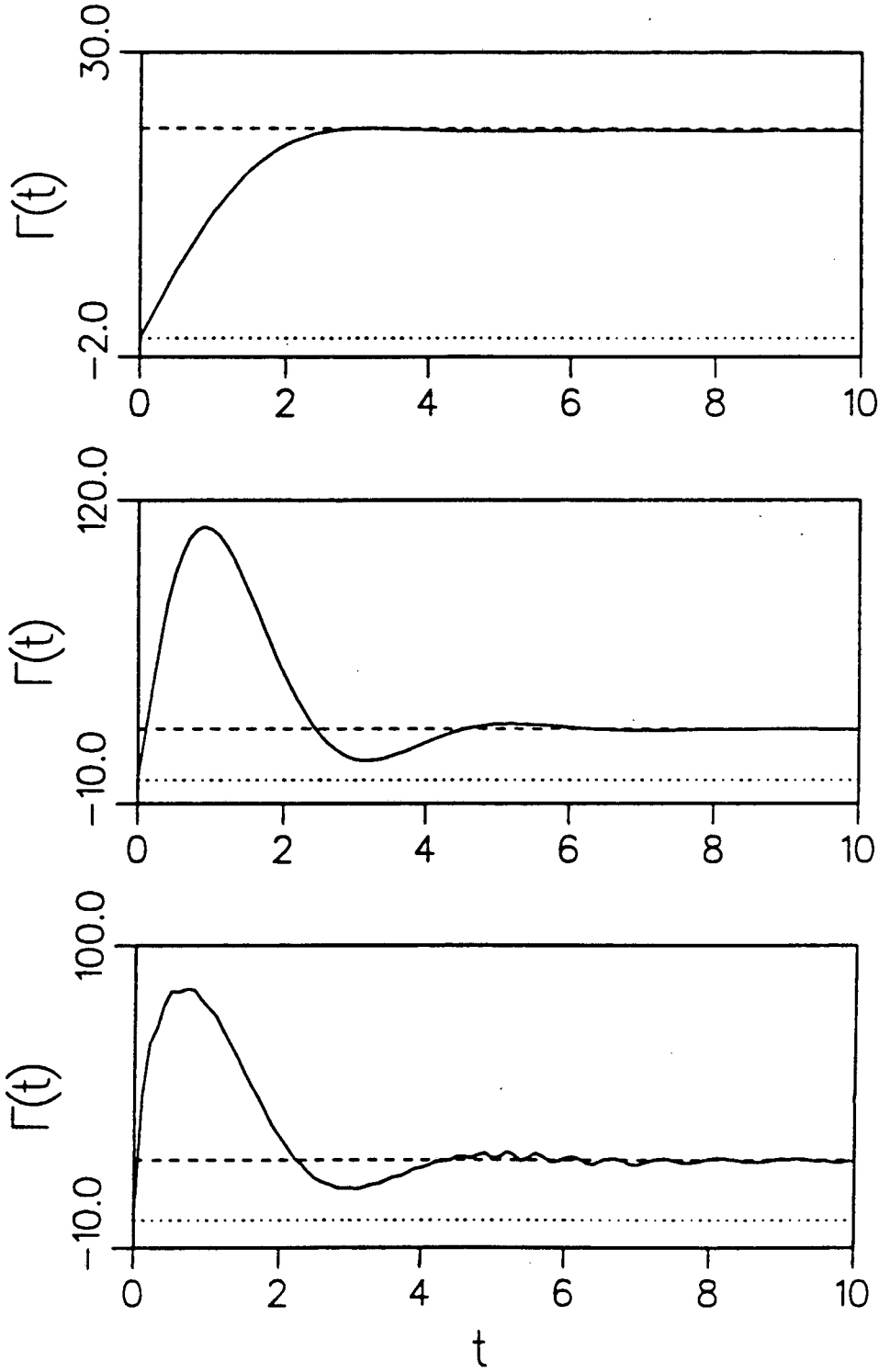

FIGURE 9

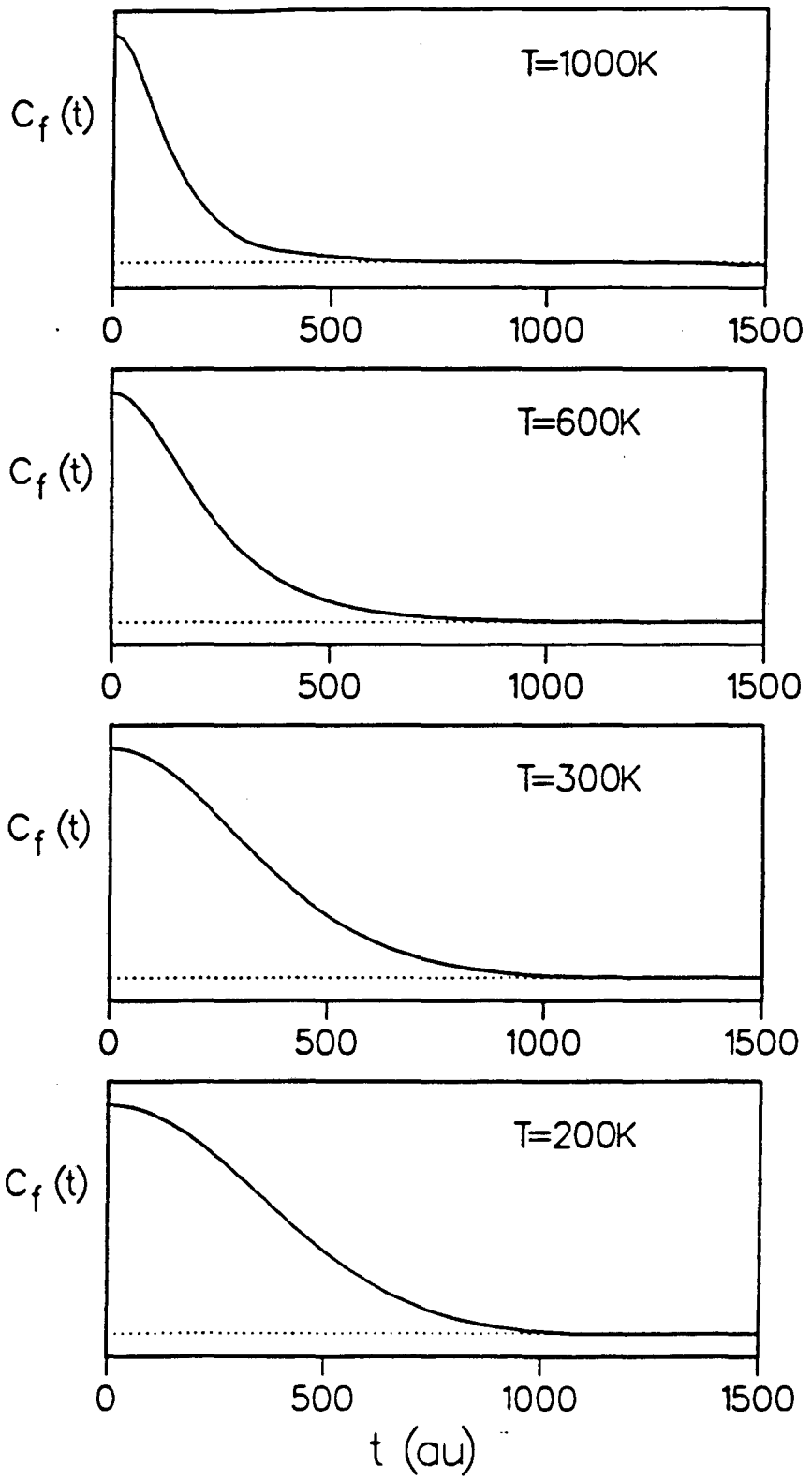
T=1000K
C_f (t)
0
500
1000
1500
T=600K
C_f (t)
0
500
1000
1500
T=300K
C_f (t)
0
500
1000
1500
T=200K
C_f (t)
0
500
1000
1500
t (au)

FIGURE 10

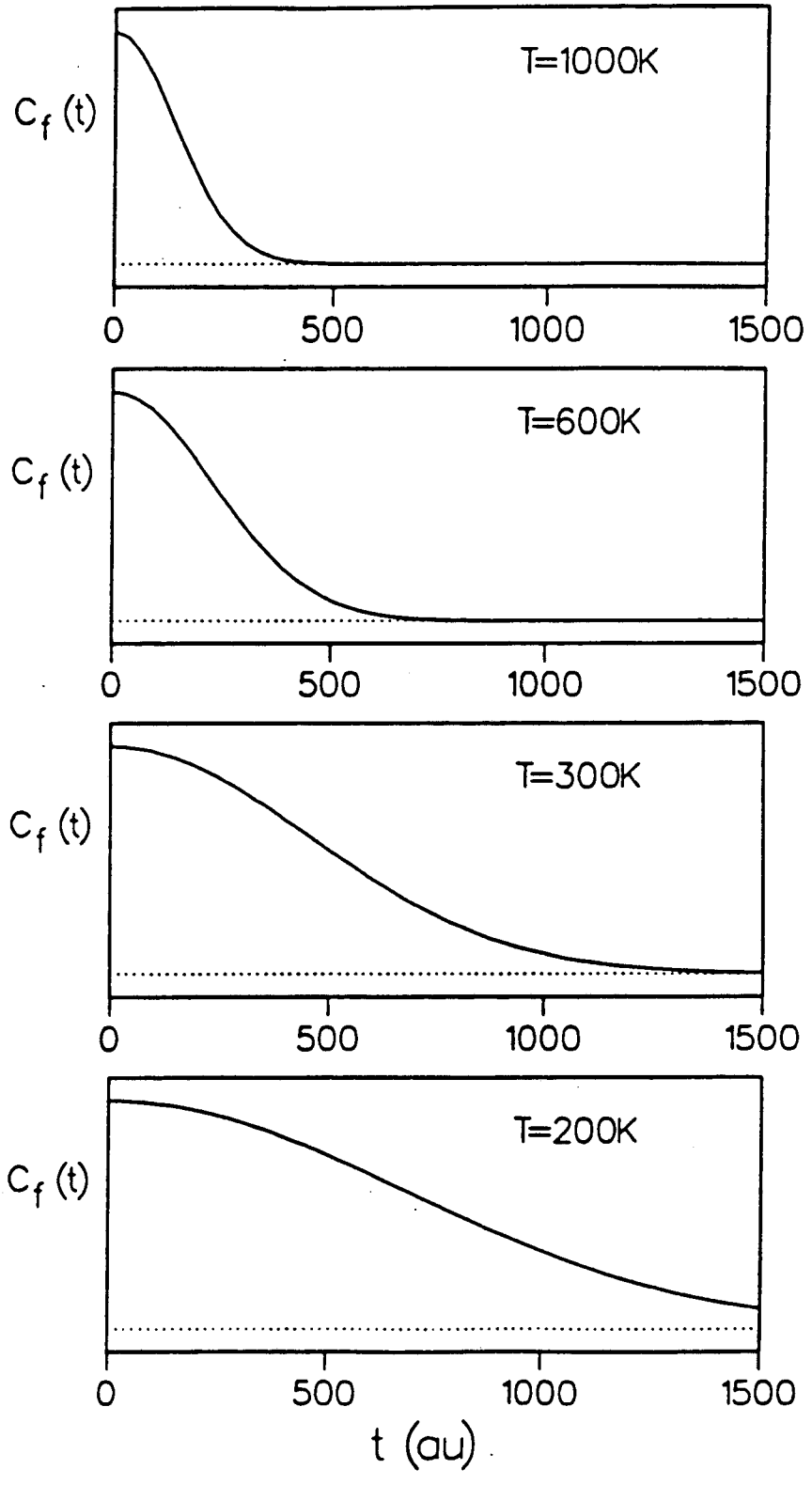
T=1000K
C_f (t)
0
500
1000
1500
T=600K
C_f (t)
0
500
1000
1500
T=300K
C_f (t)
0
500
1000
1500
T=200K
C_f (t)
0
500
1000
1500
t (au)

FIGURE 11

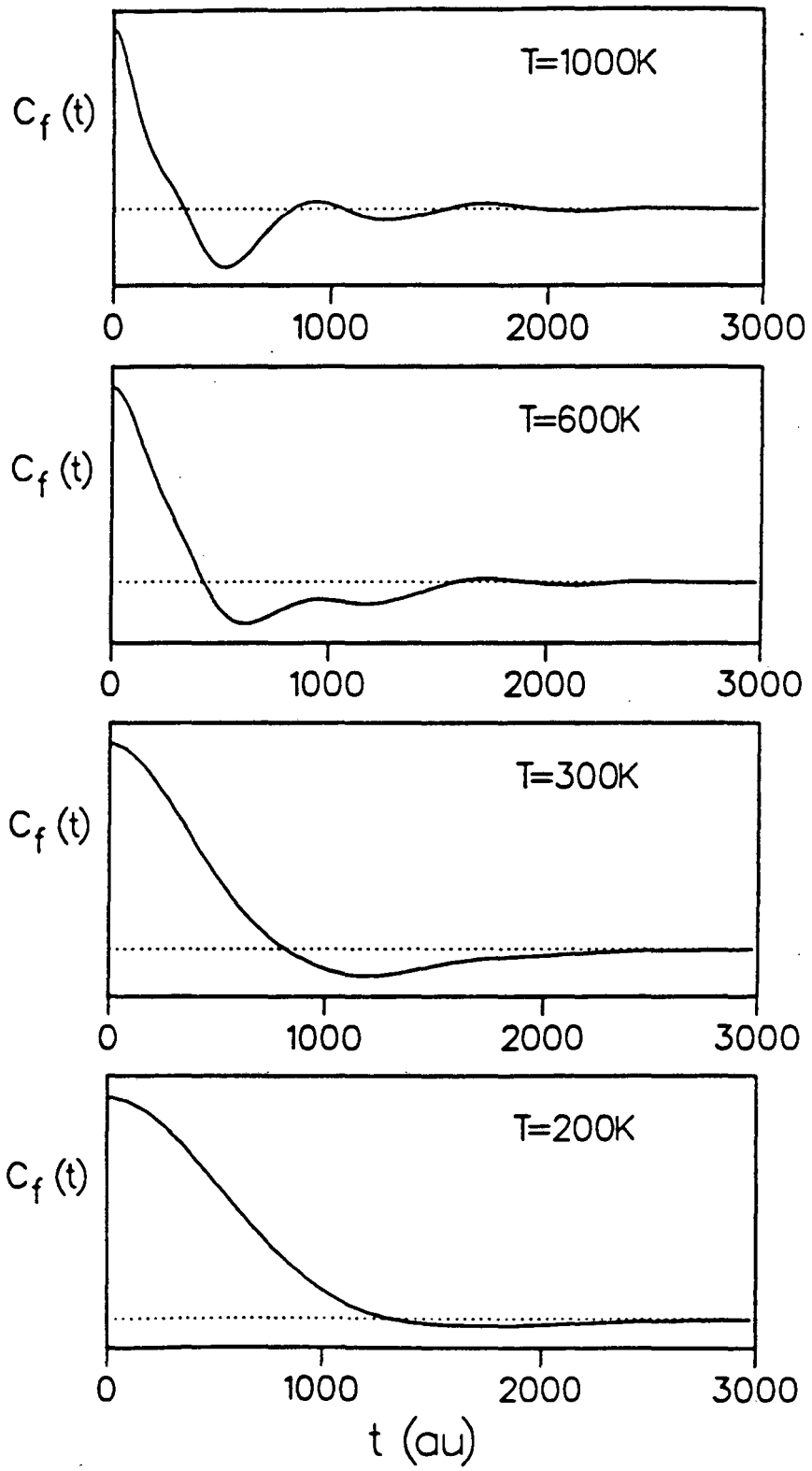
T=1000K
C_f (t)
0
1000
2000
3000
T=600K
C_f (t)
0
1000
2000
3000
T=300K
C_f (t)
0
1000
2000
3000
T=200K
C_f (t)
0
1000
2000
3000
t (au)

FIGURE 12

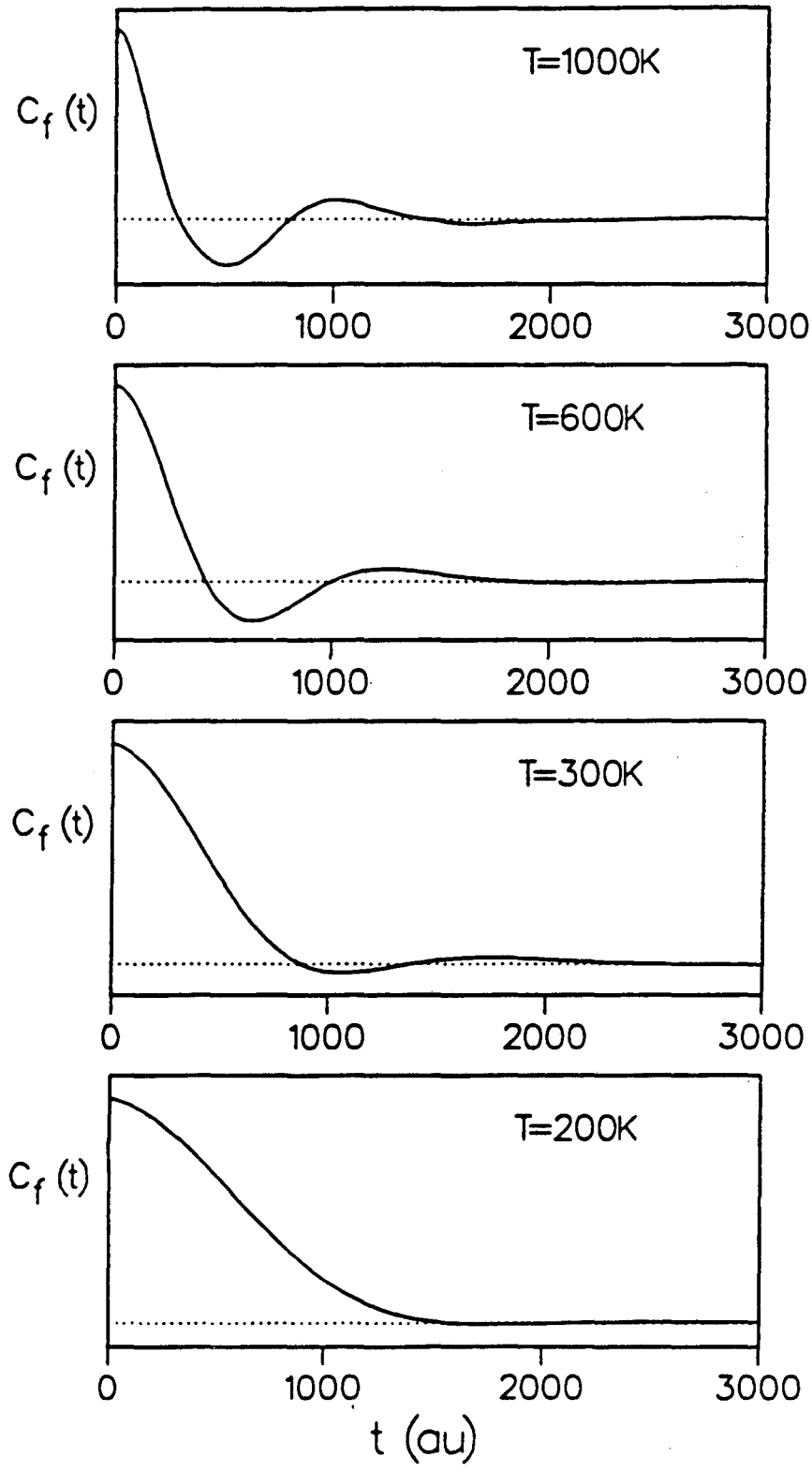
T=1000K
C_f (t)
0
1000
2000
3000
T=600K
C_f (t)
0
1000
2000
3000
T=300K
C_f (t)
0
1000
2000
3000
T=200K
C_f (t)
0
1000
2000
3000
t (au)

FIGURE 13

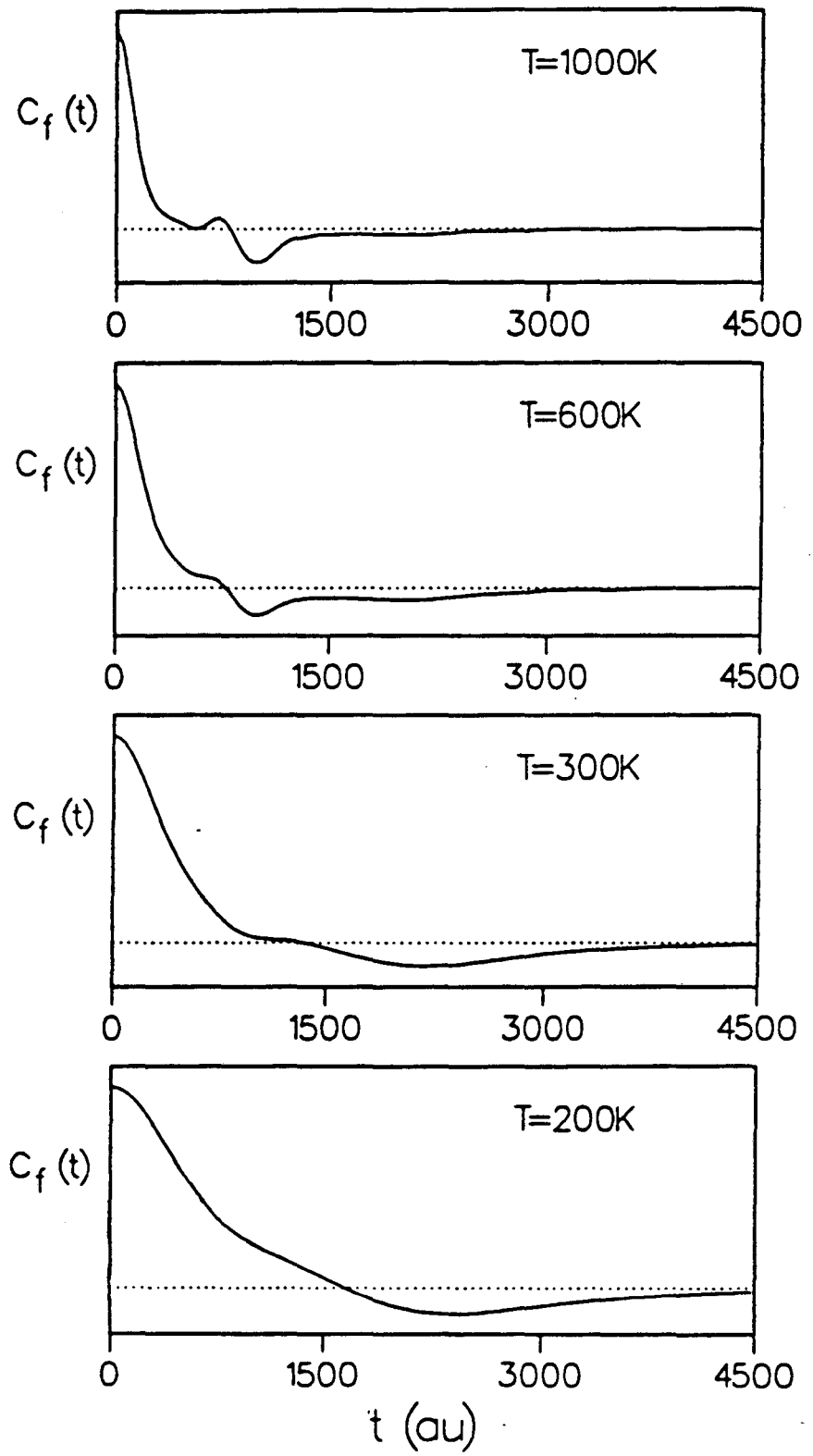
T=1000K
C_f (t)
0
1500
3000
4500
T=600K
C_f (t)
0
1500
3000
4500
T=300K
C_f (t)
0
1500
3000
4500
T=200K
C_f (t)
0
1500
3000
4500
t (au)

FIGURE 14

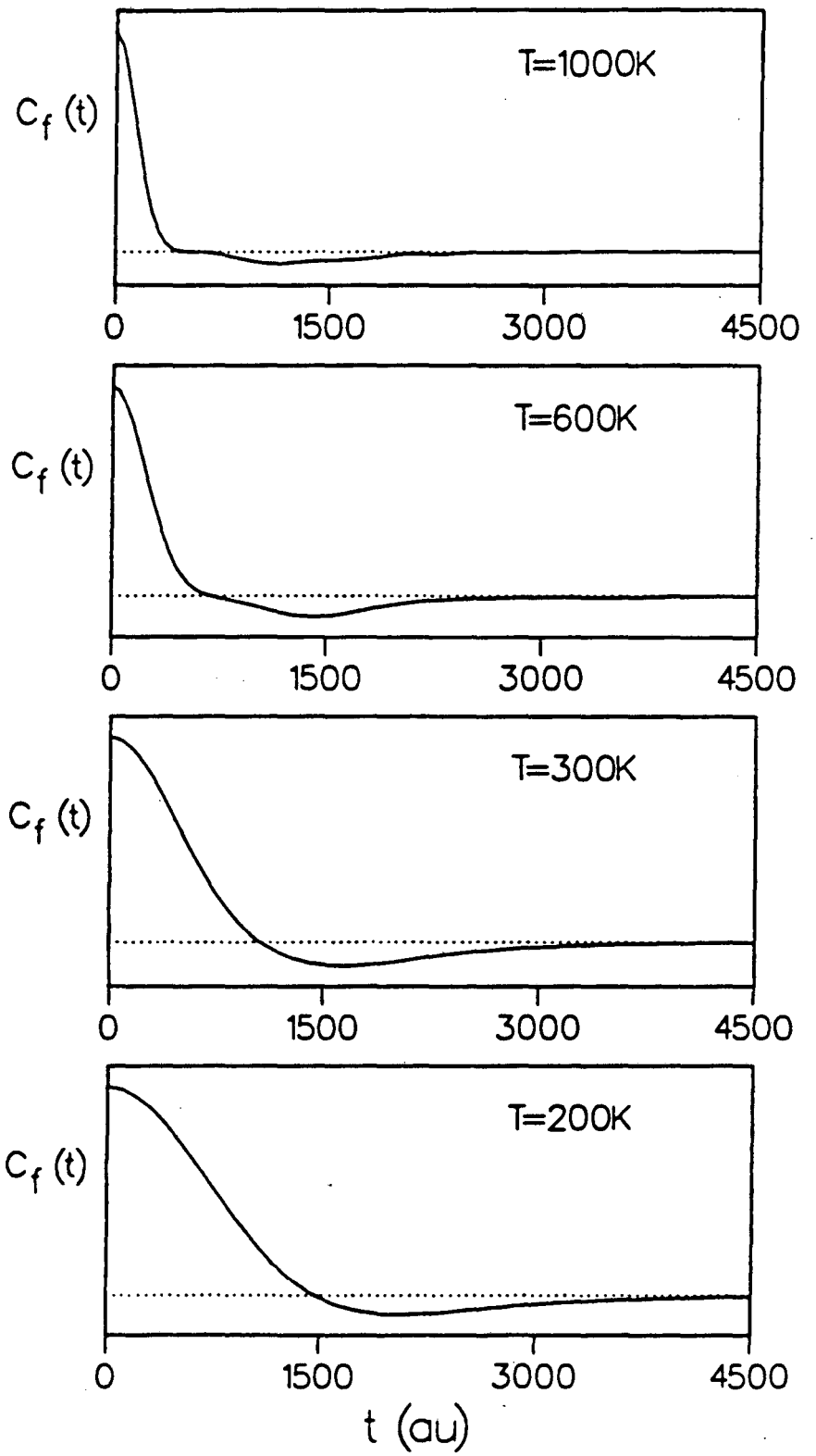
T=1000K
C_f (t)
0
1500
3000
4500
T=600K
C_f (t)
0
1500
3000
4500
T=300K
C_f (t)
0
1500
3000
4500
T=200K
C_f (t)
0
1500
3000
4500
t (au)

FIGURE 15

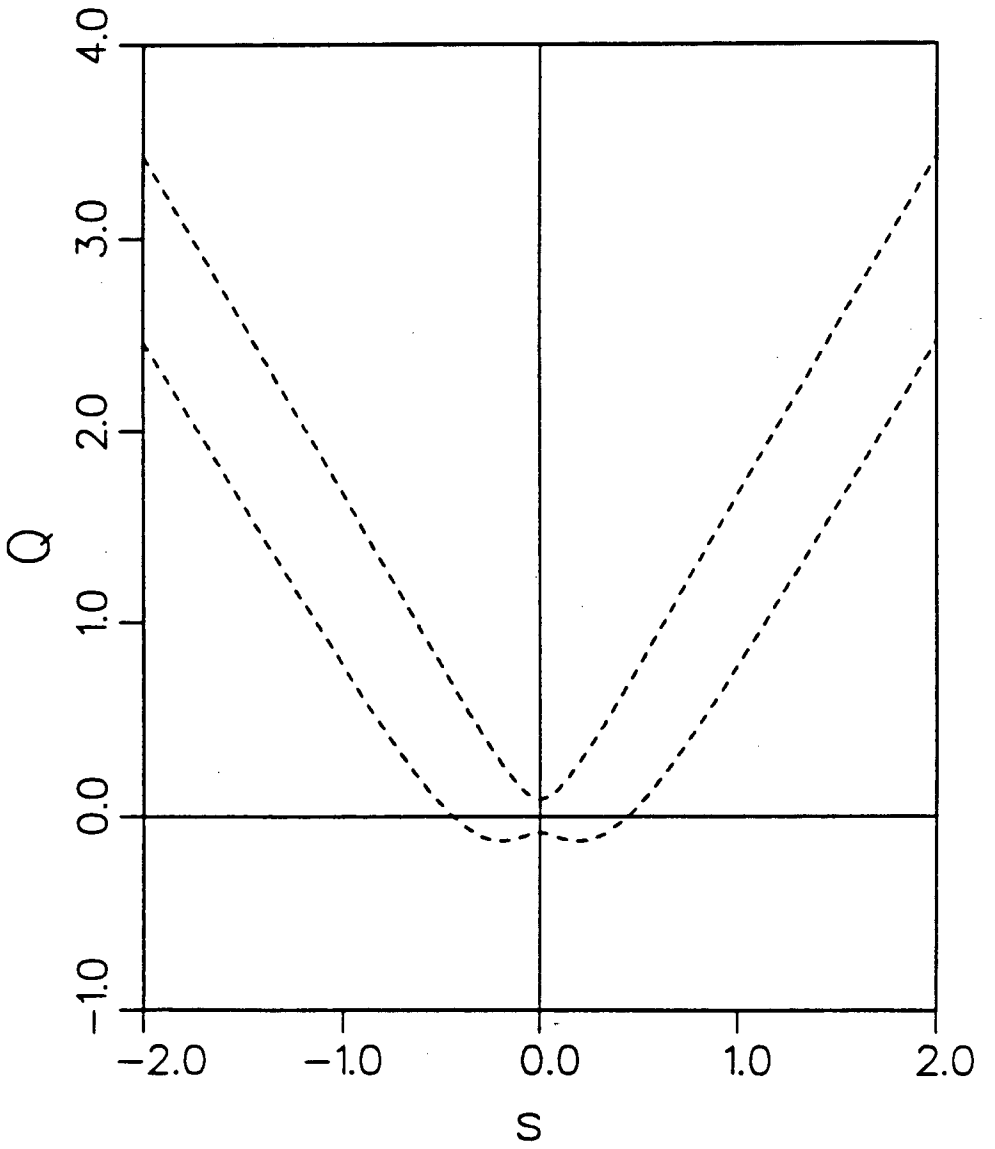

FIGURE 16

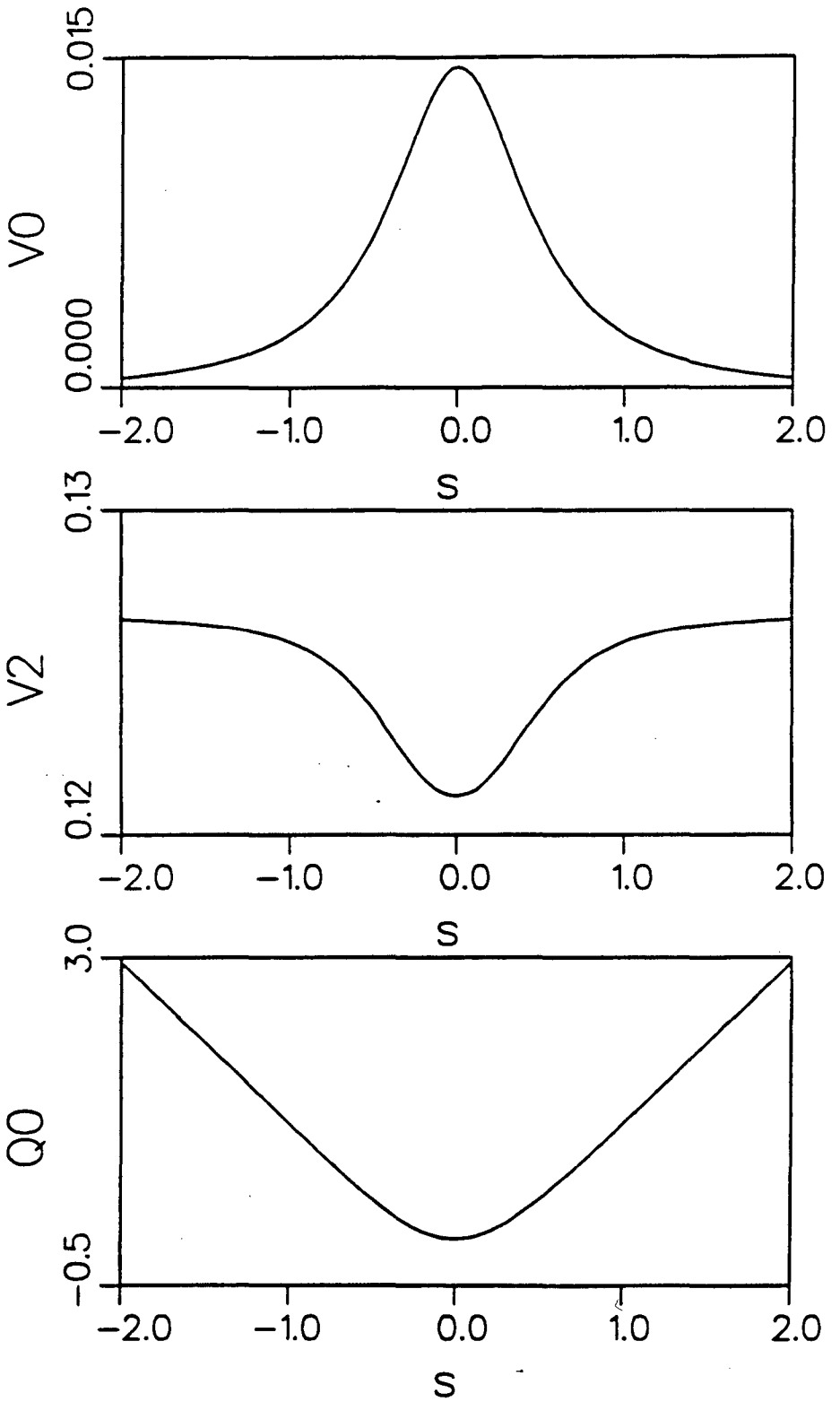
0.015
0.000
V0
−2.0
−1.0
0.0
1.0
2.0
S
0.13
0.12
V2
−2.0
−1.0
0.0
1.0
2.0
S
3.0
−0.5
Q0
−2.0
−1.0
0.0
1.0
2.0
S

LAWRENCE BERKELEY LABORATORY
TECHNICAL INFORMATION DEPARTMENT
UNIVERSITY OF CALIFORNIA
BERKELEY, CALIFORNIA 94720